

# QUILL

## Quarterly Reports



August - October 2021



All information held within is confidential and is

Copyright © QUILL 2021.

It contains proprietary information which is disclosed for information purposes only.

The contents shall not in whole or in part

(i) be used for other purposes,

(ii) be disclosed to any person not being a member of staff or student of QUILL

(3 year period up to November 2024)

(iii) be disclosed to any person not being a member of staff of a QUILL industry member or one of their affiliated companies,

(iv) be stored in any retrieval system, or reproduced in any manner which does not fulfil conditions (i), (ii) and (iii) without the written permission of the Director of QUILL, The Queen's University of Belfast, David Keir Building, Stranmillis Road, Belfast BT9 5AG, United Kingdom.



## Contents

Design of New, Non-coordinating, and Hydrophobic Anions for Functional Ionic Liquids (Haris Amir).....	4
Recycle and Reuse of Process Water Through Sulfate Removal: Developing an Ionic Liquid Technology for Selective Anion Recognition and Extraction (Dominic Burns).....	8
Battery Thermal Management and Algorithmic 3D Temperature Prediction (Andrew Forde).....	10
Mechanism Understanding of NO <sub>x</sub> storage, release and reduction on Pt/doped ceria catalysts (Oisin Hamill).....	11
Frustrated Lewis acid/base pairs in Ionic Liquids (Aloisia King) .....	13
Design of supported ionic liquid catalysts for the synthesis of 5-substituted tetrazoles to be used as draw fluids for forward osmosis in water desalination (Sanskrita Madhukailya) .....	14
Design and Development of an Effective and Interconnected Smart Fire Suppression System for Lithium-ion Batteries in Electric Vehicles (David McAreavey).....	19
Chemisorbent materials for olefin and paraffin separation (Sam McCalmont).....	21
Acidic Ionic Liquids As Catalysts For The Valorisation Of Waste Plastic Resource (Emma McCrea).....	23
Boron Lewis acids: structure and applications (Anne McGrogan).....	24
Pressure-induced liquid-liquid transition in a family of ionic materials (Shannon McLaughlin).....	29
Redox Flow Battery Materials for Energy Storage (Hugh O'Connor) .....	34
Molecular Electrocatalysts for Energy and Electrosynthetic Applications (Scott Place) .....	35
Use ionic liquids that exhibit LCST (lower critical solution temperature) behaviour as draw fluids for water treatment, desalination and separation (Junzhe Quan).....	36
Thermochemical Conversion of Biomass Lignin into Mesoporous Carbon Materials (Yaoguang Song) .....	39
Modelling the use of Flow Batteries in Transport Applications (Richard Woodfield).....	47
Gas separation technologies (Mark Young).....	48

## QUILL Quarterly Report

August 2021 – October 2021

<b>Name:</b>	Haris Amir		
<b>Supervisor(s):</b>	Prof John Holbrey		
<b>Position:</b>	Postgraduate (PhD)		
<b>Start date:</b>	01/10/2020	<b>Anticipated end date:</b>	30/09/2023
<b>Funding body:</b>	ESPRC/UKRI		

### Design of New, Non-coordinating, and Hydrophobic Anions for Functional Ionic Liquids

New boron containing anions are of interest for the development of new ionic liquid anions with a wide range of potential applications including electro- and photo- chemistry, and for the separation and extraction of metals and waste. In this work, functional borate anions formed as complexes with O/N-chelators for ionic liquid applications have been designed and investigated.

A more efficient synthesis of different alkali salt borate anions incorporating O- and N/O- donor ligands is described. Anion exchange is performed with tetrabutylphosphonium chloride  $[P_{4444}]Cl$  to obtain ionic liquids with  $[P_{4444}]^+$  cations combined with the different borate anions. In a number of cases, the tetrabutylphosphonium salts could be crystallised allowing single crystal XRD studies to be performed.

#### New synthetic approach to alkali salt borate anions

The previous strategy described to generate borate ionic liquids for investigation was to synthesise the free acid of the borate anion (figure 1) followed by neutralisation with a base, in this case potassium hydroxide was chosen. This gave the desired 4-coordinate borate anion as a potassium salt. This was then used in an anion exchange reaction with tetrabutylphosphonium chloride  $[P_{4444}]Cl$  to obtain ionic liquids with the newly developed borate anions.

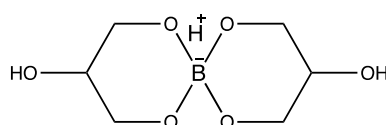


**Figure 1** -Structure of the free acid borate anion.

The yield of the obtained salts was a high average of 82.3% however, an efficient synthetic approach was reported for the synthesis of bis(salicylato)borate (BScB) salt. It was reported that the use of  $Na_2CO_3$  aqueous solution with 1 mol of boric acid and 2 mol of salicylic acid directly results in the synthesis of  $Na[BScB]$  with a yield of 85%. This synthetic approach was repeated to directly generate sodium salts of the borate anions incorporating O- and N/O- donor ligands, shown in table 1 without requiring initial formation of the acid – which have previously been shown to be labile, exchanging with three-coordinate neutral boron species.

**Table 1** - The  $\delta^{11}\text{B}$  NMR of the borate ester anions before and after the addition of  $\text{Na}_2\text{CO}_3$

Borate ester	$\delta^{11}\text{B}$ NMR (ppm)	Na salt of borate ester	$\delta^{11}\text{B}$ NMR (ppm)
$[\text{H}][\text{B}(\text{gly})_2]$	19.38	$\text{Na}[\text{B}(\text{gly})_2]$	5.23
$[\text{H}][\text{B}(\text{C}_4\text{H}_8\text{O}_2)_2]$	18.14	$\text{Na}[\text{B}(\text{C}_4\text{H}_8\text{O}_2)_2]$	3.03
$[\text{H}][\text{B}(\text{C}_2\text{H}_4\text{O}_2)_2]$	18.56	$\text{Na}[\text{B}(\text{C}_2\text{H}_4\text{O}_2)_2]$	3.18
$[\text{H}][\text{B}(\text{C}_4\text{H}_9\text{NO})_2]$	14.56	$\text{Na}[\text{B}(\text{C}_4\text{H}_9\text{NO})_2]$	2.21
$[\text{H}][\text{B}(\text{C}_3\text{H}_7\text{NO})_2]$	19.56	$\text{Na}[\text{B}(\text{C}_3\text{H}_7\text{NO})_2]$	2.55
$[\text{H}][\text{B}(\text{C}_3\text{H}_7\text{NO})_2]$	19.42	$\text{Na}[\text{B}(\text{C}_3\text{H}_7\text{NO})_2]$	2.06
$[\text{H}][\text{BScB}]$	-	$\text{Na}[\text{BScB}]$	3.42

The results in table 1 show that this approach was successful in forming the desired 4-coordinate borate anion as a Na salt, as all showed a sharp peak in the  $^{11}\text{B}$  NMR in the region of 4-coordinate borate anions. The average yield increased slightly from 82.3% to 84.7%, this along with the fact the synthesis is easy to scale, and repeat resulted in adopting this more efficient synthetic approach in the future.

### Synthesis of $[\text{P}_{4444}]^+$ based ionic liquid

Once the synthesis of Na salt was adopted, the next step was to perform anion exchange to obtain phosphonium based ionic liquids and perform single crystal XRD to confirm the presence of these 4-coordinate borate anions. The obtained  $\text{Na}[\text{BScB}]$  was mixed with  $[\text{P}_{4444}]\text{Cl}$  in chloroform and left to stir, the organic layer was washed with deionised water. The chloroform was removed, and the product was dried under reduced pressure at  $70^\circ\text{C}$ , this resulted in beige crystals. The  $^{31}\text{P}\{^1\text{H}\}$  and  $^{11}\text{B}$  NMR shown in figure 2a and 2b respectively shows a single peak as expected.

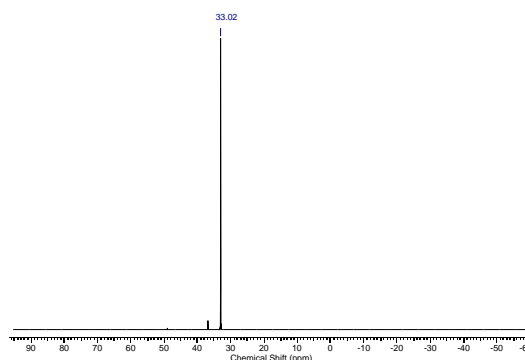


**Figure 2a** -  $^{31}\text{P}\{^1\text{H}\}$  of  $[\text{P}_{4444}][\text{BScB}]$

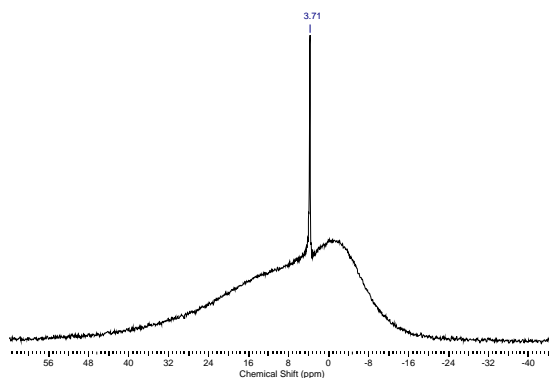


**Figure 2b** -  $^{11}\text{B}$  of  $[\text{P}_{4444}][\text{BScB}]$

The  $^1\text{H}$  and  $^{13}\text{C}$  NMR (figure 3a and 3b respectively) shows the presence of both the phosphonium cation and the borate anion suggesting the anion exchange was successful. However, there are also the presence of small unidentified peaks in the  $^1\text{H}$  NMR, this could mean the ionic liquid is not completely pure and attempts of purifying and recrystallising the ionic liquid will be made.

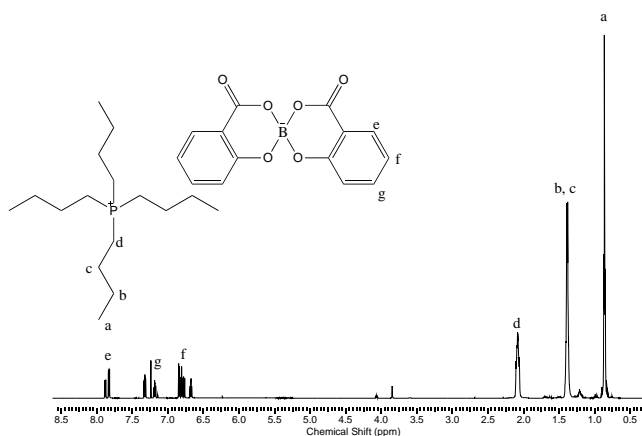


**Figure 3a** -  $^1\text{H}$  of  $[\text{P}_{4444}][\text{BScB}]$

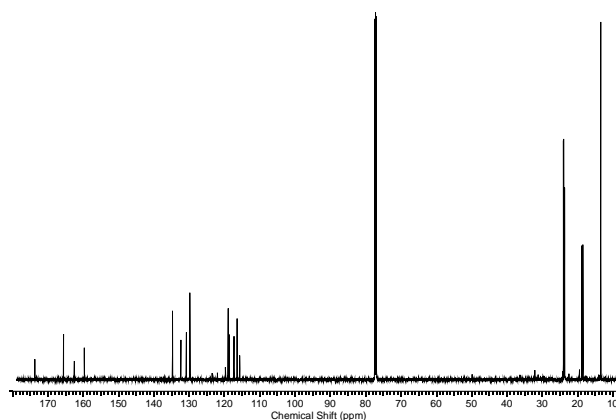


**Figure 3b** -  $^{13}\text{C}$  of  $[\text{P}_{4444}][\text{BScB}]$

Despite the impurities shown in the NMR, single crystal XRD was run in attempt to confirm the presence of the 4-coordinate borate anion. The obtained crystal structure is illustrated below in

figure 4. The crystal structure validates what the NMR shows, that being the presence of the 4-coordinate boron anion. The bond length between the boron centre and the 4 oxygen atoms varies with the longest being 1.472 Å and the shortest being 1.441 Å, these differences in bond length from the centre may explain why B-O bonds are labile. Further single crystal XRD will be run for the remaining 4-coordinate boron anions shown in Table 1.

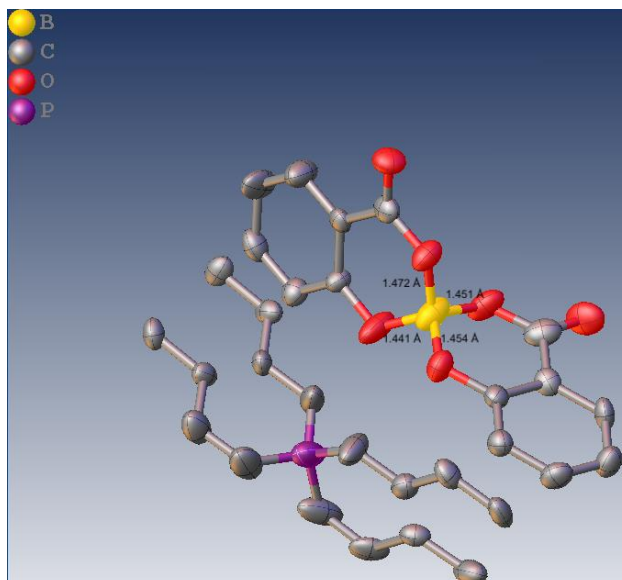


**Figure 4** - Crystal structure of  $[P_{4444}][BScB]$

## QUILL Quarterly Report

August 2021 – October 2021

<b>Name:</b>	Dominic Burns		
<b>Supervisor(s):</b>	Prof John Holbrey, Dr Gosia Swadzba-Kwasny and Dr Hye-Kyung Timken		
<b>Position:</b>	PhD Student		
<b>Start date:</b>	1 <sup>st</sup> October 2019	<b>Anticipated end date:</b>	31 <sup>st</sup> May 2023
<b>Funding body:</b>	EPSRC		

### Recycle and Reuse of Process Water Through Sulfate Removal: Developing an Ionic Liquid Technology for Selective Anion Recognition and Extraction

This is an EPSRC industrial CASE project in collaboration with Chevron, to explore liquid technologies for the treatment of saline process water with the initial objective of selective sulfate removal from highly competitive aqueous streams. Initial work began by characterising [P66614]Cl as a liquid anion exchanger. This work showed that sulfate can be extracted by [P66614]Cl from 'ideal' sodium sulfate solutions via anion exchange as shown in the graph below. However, when chloride is already present in the aqueous phase this blocks the exchange process reducing the extraction to almost zero. The current main approach is a liquid-liquid extraction where sulfate specific receptors are dissolved into the IL phase which can then bind to the sulfate. Other approaches currently on pause include micelle forming receptors that have previously been reported on and thiuronium ILs that are known to be good moieties for anion complexation.

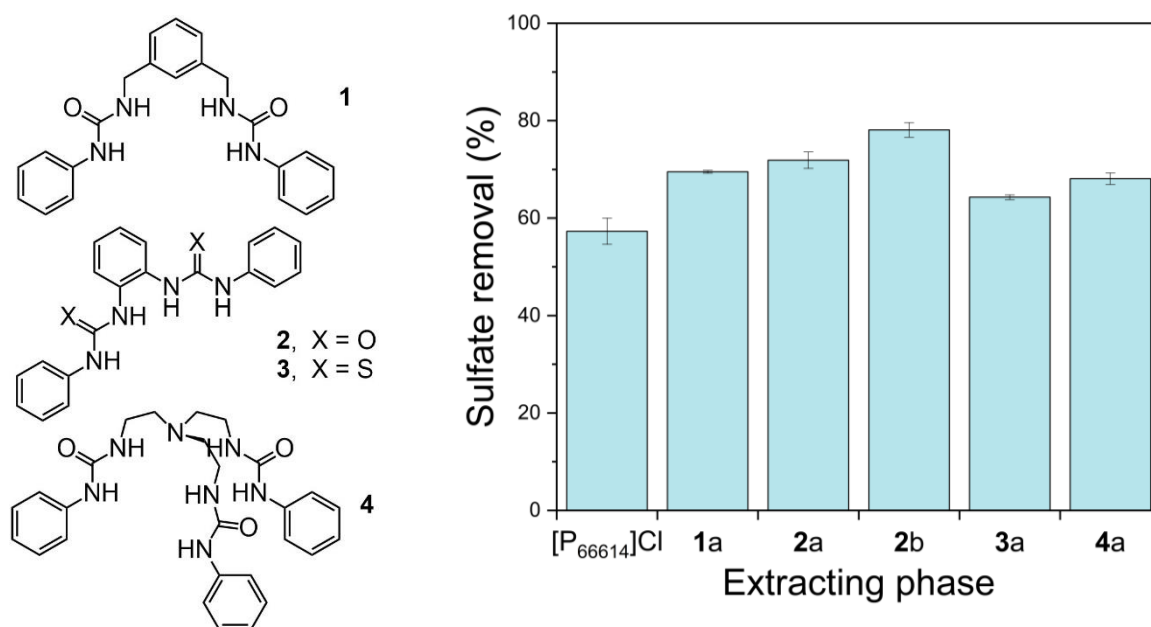


**Figure 1** - Anion receptors used so far in this work (left) and their ability to enhance the removal of sulfate from an 'ideal' 2,600 ppm aqueous solution (right), where a = 56.4 mM (1 equiv), b = 108.2 mM (2 equiv).



Furthering research from the last quarter where receptors **1** - **3** had been synthesised and tested for their potential to act as additives to  $[P_{66614}]Cl$  to enhance the removal of sulfate via an ion-exchange process. Receptor **4** has now also been synthesised and tested as well as a thiourea analogue of receptor **4** (synthesised but not yet tested). While receptor **4** is reported to have a much larger sulfate binding constant than the previously tested receptors ( $K_a > 10,000$  from DOI: 10.1021/ja205884y), its performance was slightly worse than receptors **1** and **2**. This is thought to be due to its also increased binding affinity for the chloride ( $K_a = 882$ ) creating a much larger energy barrier for the ion-exchange process.

Previous results where it was shown that some of these receptors had potential to removed nearly 10% of sulfate from sea water has since been disproven and found to be due to an inaccurate calibration of the ED-XRF machine. New calibrations have since been generated and it was found that the analysis is more accurate if 'ideal' and sea water samples are measured with separate calibrations.

Binding studies in DMSO as well as in  $[P_{66614}]Cl$  are currently being conducted to investigate the binding of these receptors with sulfate and chloride and to help understand why the enhancements do not seem proportional to the ability of each receptor to bind sulfate.

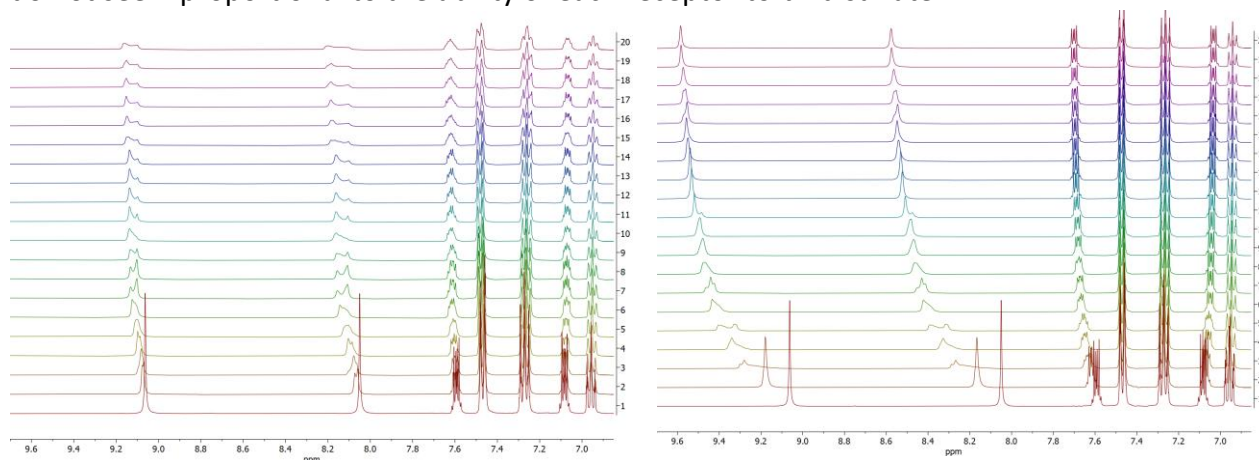


**Figure 2** -  $^1H$  NMR titration studies of receptor **2** with sulfate (left) and chloride (right) in  $DMSO-d_6$ . Concentration of guest ranges from 0 to 6 equivalents with respect to the host concentration

So far receptor **2** has been studied via  $^1H$  NMR titration in DMSO with sulfate and chloride as shown below. In these studies, the concentration of host (**2**) is kept constant and small portions of guest are added with  $^1H$  NMR run after each addition to show the degree of complexation between the host and guest from 0 to 6 equivalents of guest in solution.

The binding constant with chloride was determined to be  $55.99 M^{-1}$ , slightly smaller than the published value of  $63 M^{-1}$  (from DOI: 10.1021/ja205884y) and the sulfate binding constant was determined to be  $24.75 M^{-1}$  which has not been determined in the literature. Interesting that even though this suggests **2** binds chloride much stronger than it does sulfate, it can still enhance the sulfate-chloride ion exchange process by 20%. Further studies are now being conducted in  $[P_{66614}]Cl$  which provides a drastically different environment than DMSO and will hopefully help understand this enhancement.



## QUILL Quarterly Report

August 2021 – October 2021

<b>Name:</b>	Andrew Forde		
<b>Supervisor(s):</b>	Dr Stephen Glover, Dr Rob Watson and Prof Peter Nockemann		
<b>Position:</b>	PhD Student		
<b>Start date:</b>	03/06/2019	<b>Anticipated end date:</b>	03/12/22
<b>Funding body:</b>	Horiba-MIRA & EPSRC		

### Battery Thermal Management and Algorithmic 3D Temperature Prediction

#### Experimental

A collaboration has been established with University College London. Work has been carried out in the battery group of UCL involving acoustic measurements for monitoring of SOC and temperature. As this project is interested in internal battery temperature, these methods are well suited for model parameterisation and validation. Therefore, the commercial cells to be used for this project were sent to UCL for acoustic measurements. These measurements have now been taken and transport is being organised to move the cells to QUB for the remainder of the experimental work.

#### Numerical Model

A 3D numerical model for battery simulation is being designed for the purpose of temperature prediction. Various methods of optimisation have been explored and new input methods implemented for better generalisation between various cell chemistries and geometry.



## QUILL Quarterly Report

August 2021 – October 2021

<b>Name:</b>	Oisin Hamill		
<b>Supervisor(s):</b>	Dr Nancy Artioli and Dr Alex Goguet		
<b>Position:</b>	PhD		
<b>Start date:</b>	01/10/2019	<b>Anticipated end date:</b>	30/09/2022
<b>Funding body:</b>	EPSRC		

### Mechanism Understanding of NO<sub>x</sub> storage, release and reduction on Pt/doped ceria catalysts

#### Background

Due to strengthening emission legislations in Europe, North America and the rest of the world, there is a need for further optimisation of existing emission after-treatment catalytic converters for automotive applications. New legislations focus primarily of NO<sub>x</sub> abatement and consequently the exhaust emissions of lean-burn gasoline and diesel vehicles. After treatments systems must utilise new technologies to reduce this that offer low temperature activation and high stability.

High surface area ceria is successfully employed as an excellent support of metals (Pd, Rh, Pt, etc.) in commercial catalytic systems for the oxidations of carbon monoxide and propane and automotive emission control. Ceria is a unique material with a rich and complex chemistry. It possesses high oxygen storage capacity (OSC), a unique redox property by the cycle of Ce<sup>4+</sup>/Ce<sup>3+</sup> redox pairs and it can be further enhanced through using dopants. Platinum supported on ceria can show enhanced NO<sub>x</sub> storage at low temperature, as reported in the literature, together with an improved carbon monoxide/hydrocarbon light off.

Ceria supported catalysts, in general, do not operate efficiently at low temperatures and therefore must be modified in order to overcome this problem. For this reason, addition of enhancing materials is currently being considered in detail. This addition of a material that increases the performance of an already functional catalyst is called doping. The main function of this dopant is to allow the catalyst to function outside of the normal working temperature range and operating conditions to increase catalyst efficiency.

It has been proposed that the dopants, such as rare-earth and transition metal oxides, increase the concentration of surface vacancies which affect the ionic conductivity, oxygen mobility and oxygen storage capacity of the ceria. It can be speculated that all these properties are responsible for the enhanced oxidation activity by promoting oxygen diffusion and formation of more "reactive oxygen" species. Furthermore, the oxygen species play a role in the mechanism of the reaction, favouring the NO<sub>x</sub> storage. Additionally, presence of dopants can reportedly modify the platinum reducibility and platinum-ceria interaction, allowing more readily activation during rich purge.

This project aims to better understand the NO<sub>x</sub> storage mechanism on the doped materials and give new insights into the activation/lean deactivation mechanisms in the presence of different dopants.



### **Objective of this work**

The main objective considered in this project is to improve the understanding of the NO<sub>x</sub> storage mechanism, together with the mechanism of rich purge on ceria supported platinum. We aim to gain a deeper knowledge of the rich activation and lean deactivation mechanisms as well as determine the structure of the active sites under reaction conditions. We look to develop a method to differentiate between active species and spectator species through transient methods. We will also strive to develop a global kinetic model for the reaction and all involved species. This will enable the determination of the relative importance of different reactions within the catalyst bed as well as a measurement of the exact gas compositional conditions present during the reactions. With this approach in depth information relevant to mechanistic understanding and reaction engineering application will be obtained.

### **Progress to date**

- TPR results for all Sm doped samples.
- Lean/Rich cyclic experiments completed for Sm doped and undoped ceria based catalysts.
- NO<sub>x</sub> Storage Capacity Tests began for Sm doped catalyst.
- NAM27 Abstract Submitted

### **Conclusions and future work**

- NSC tests for all doped and undoped catalysts including new dopants.
- Lean/Rich cyclic experiments for Nd to be repeated to compare directly to Sm doped results.
- Characterisation on new dopants & dopant oxides.
- UKCC Abstract to submit.
- In-Situ & Ex-Situ EXAFS results to be proposed and studied.
- XPS results to be studied and further catalysts to be characterised, prioritising Sm doped catalysts.



## QUILL Quarterly Report

August 2021 – October 2021

<b>Name:</b>	Aloisia King		
<b>Supervisor(s):</b>	Prof John Holbrey and Prof Gosia Swadzba-Kwansy		
<b>Position:</b>	PhD student		
<b>Start date:</b>	01/10/2021	<b>Anticipated end date:</b>	March 2024
<b>Funding body:</b>	EPSRC		

### Frustrated Lewis acid/base pairs in Ionic Liquids

To date I have been doing extensive literature research in order to understand my project in more thorough detail and the potential applications that the research could have. It was decided that I would first synthesise a range of pyridine [NTf<sub>2</sub>] ionic liquids and hence test the solubility and behaviour of a range of N-alkyl acridinium salts. So far the synthesis of the ILs is going well and I have successfully synthesised Lutidinium bistrisulfonylimide [Lut-H]<sup>+</sup> [NTf<sub>2</sub>]<sup>-</sup>. The IL was characterised by NMR and phase transitions and crystallisation events were recorded by DSC. The IL was synthesised on a 5mmol and 10mmol scale by anion metathesis. In literature, the Li[NTf<sub>2</sub>] was subjected to Kugelrohr distillation, which can be a time consuming procedure in order to separate the [NTf<sub>2</sub>] anion for subsequent reaction. Alternatively, the synthesis that we adopted was to neutralise the 2, 6-Lutidine by HCl in water and subsequently carry out anion metathesis by the addition of this solution to Li[NTf<sub>2</sub>]. The IL that formed was found to be miscible with water and was separated with DCM. The excess LiCl from the reaction media stayed within the aqueous layer and thereby was easy to separate. The next IL that will be synthesised will incorporate 2-Methylpyridine, instead of 2, 6-Lutidine and will follow the same procedure as previously carried out. The other pyridine molecules that will be incorporated into the IL has not yet been decided. It is the hope that we will have a series of N-alkyl acridinium salts that can be combined with this library of basic lutidine/lutidinium NTf<sub>2</sub> ionic liquid mixtures to get concentrated air stable FLP systems to test accordingly.

## QUILL Quarterly Report

August 2021 – October 2021

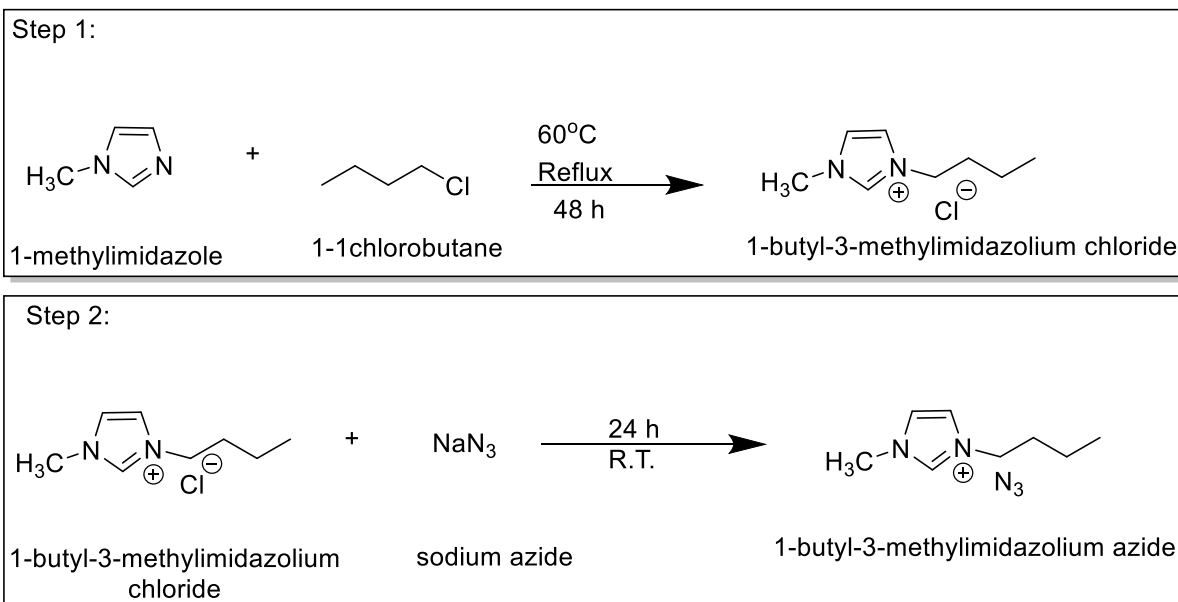
<b>Name:</b>	Sanskrita Madhukailya		
<b>Supervisor(s):</b>	Prof John Holbrey and Dr Leila Moura		
<b>Position:</b>	PhD Student (First Year)		
<b>Start date:</b>	19 <sup>th</sup> April 2021	<b>Anticipated end date:</b>	20 <sup>th</sup> April 2024
<b>Funding body:</b>	Tezpur University/QUB joint PhD scholarship		

### Design of supported ionic liquid catalysts for the synthesis of 5-substituted tetrazoles to be used as draw fluids for forward osmosis in water desalination

In the previous report, a small introduction about the research topic along with the initial objectives were mentioned, wherein the screening of catalysts for the synthesis of tetrazole was started. Following up on that, few more catalysts were screened and a convenient one was chosen. This catalyst system was then employed to make a substituted phenyl tetrazole which was further utilised in the generation of a new ionic liquid.

#### Progress to date

1. Synthesis of 1-butyl-3-methyl imidazolium azide (Fazeli, *et al.*, *ChemInform* 2014, **45**.1; Dharaskar, Swapnil A., *et al.* *The Scientific World Journal* 2013) as the azide source for the preparation of 5-phenyl tetrazole using ammonium chloride: The tetrazole was obtained in 96% yield and characterised by 1H-NMR, 13C NMR spectroscopy (Figure 1 a, b).



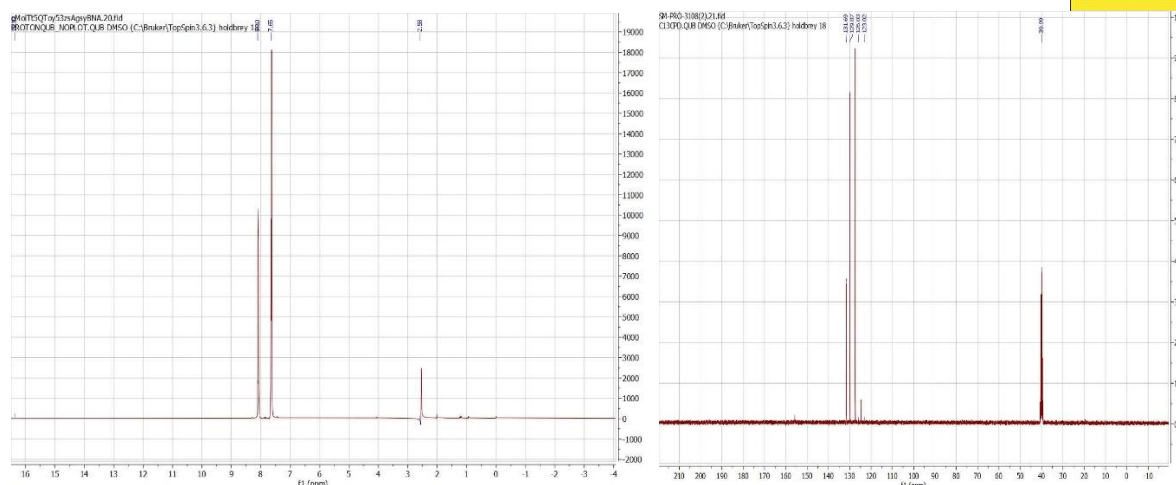


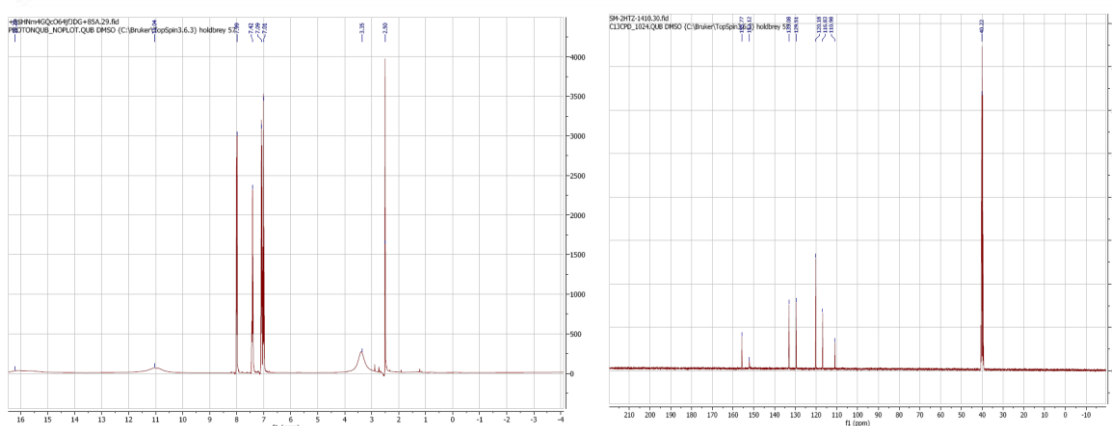
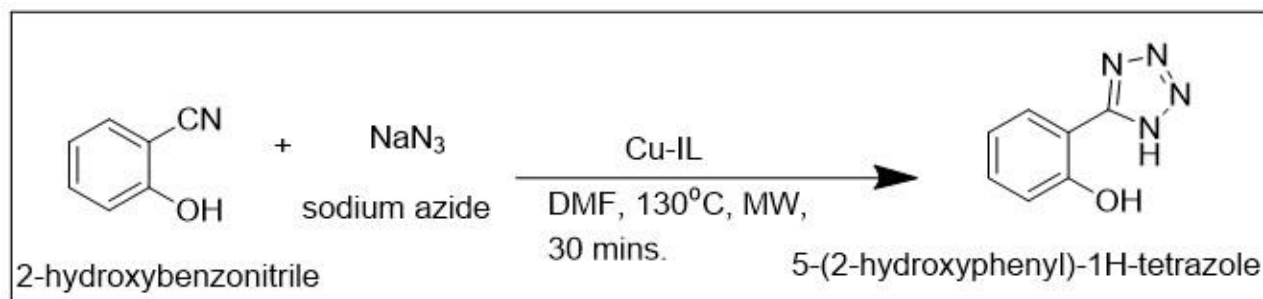
**Figure 1 a** - (left) 5-phenyl-tetrazole  $\delta^1\text{H}$  (DMSO- $\text{d}_6$ ): 16.22 (1H, N-H, tetrazole ring), 8.03-7.65 (5H, 2 peaks, phenyl ring), 2.58 (DMSO- $\text{d}_6$ ) at 50 mol%  $\text{NH}_4\text{Cl}$   
**1 b** - (right):  $\delta^{13}\text{C}$  (DMSO- $\text{d}_6$ ): 155.81 (N-C-N), 131.69-123.02 (4 peaks, phenyl ring), 39.99 (DMSO- $\text{d}_6$ ) at 50 mol%  $\text{NH}_4\text{Cl}$

2. Various other catalyst systems like L-Proline (S. B. Bhagat *et al.*, *Synlett* 2018, **29**), DMAP-Acetate (Nowrouzi *et al.*, *Tetrahedron Lett.*, 2015, **56.5**, 739-742), DIPEAc (Bhosle, M. R.; Shaikh, D. S.; Khillare, L. D.; Deshmukh, A. R.; Mane, R. A. Diisopropylethylammonium Acetate (DIPEAc): Synthetic Communications 2017, 47 (7), 695–703.), 1-disulfo-[2,2-bipyridine]-1,1-dichloride (Aali, E.; Gholizadeh, M.; Noroozi-Shad, Journal of Molecular Structure 2022, 1247, 131289), piperazinium dihydrogen sulfate (Nowrouzi, N.; Farahi, S.; Irajzadeh, M. Letters in Organic Chemistry 2016, 13 (2), 113–119) both in microwave and conventional heating were employed for the preparation of tetrazoles however, did not produce good yields.

Reaction conditions	Yield %	Overall time taken
Cu-IL/DMF	54	$\leq 50$ hours
$[\text{C}_4\text{mim}]^+\text{N}_3^-/\text{NH}_4\text{Cl}$ (50 mol%)/DMF	96	$\leq 72$ hours
$[\text{C}_4\text{mim}]^+\text{N}_3^-/\text{NH}_4\text{Cl}$ (10 mol%)/DMF	0	-do-
$[\text{C}_4\text{mim}]^+\text{N}_3^-/\text{NH}_4\text{Cl}$ (50 mol%)/DMF/MW	10	$\leq 50$ hours
$[\text{C}_4\text{mim}]^+\text{N}_3^-/\text{NH}_4\text{Cl}$ (50 mol%)/DMF:H <sub>2</sub> O (1:1)	0	$\leq 72$ hours
L-proline/DMF	0	$\leq 3$ hours
DMAP-Acetate	0	-do-

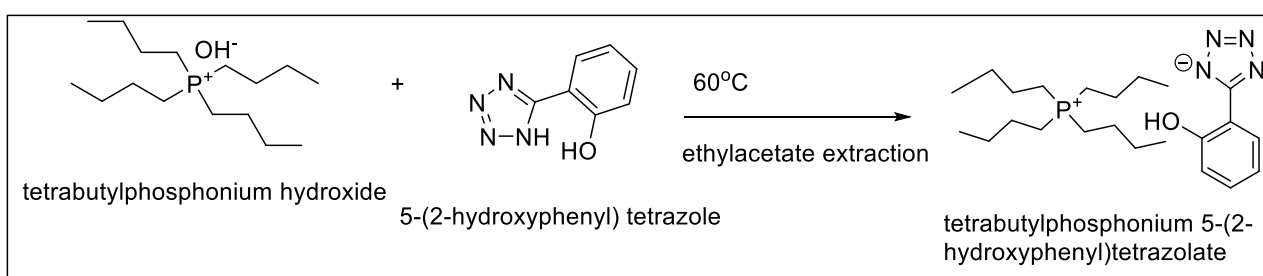
3. Considering the ease of preparation and time effectiveness of the process, the ionic liquid supported copper (II) catalyst (R. D. Padmaja *et al.*, *Res. Chem. Intermed.*, 2020, **46**, 1307–1317) was chosen as the well suited catalyst system for the preparation of tetrazoles. On that context, a

substituted tetrazole, 5-(2-hydroxyphenyl) tetrazole, a bio-isostere of salicylic acid was prepared from 2-hydroxy benzonitrile and sodium azide in good yields under microwave conditions, characterised by  $^1\text{H}$  NMR and  $^{13}\text{C}$  NMR spectroscopy (Figure 2 a, b).

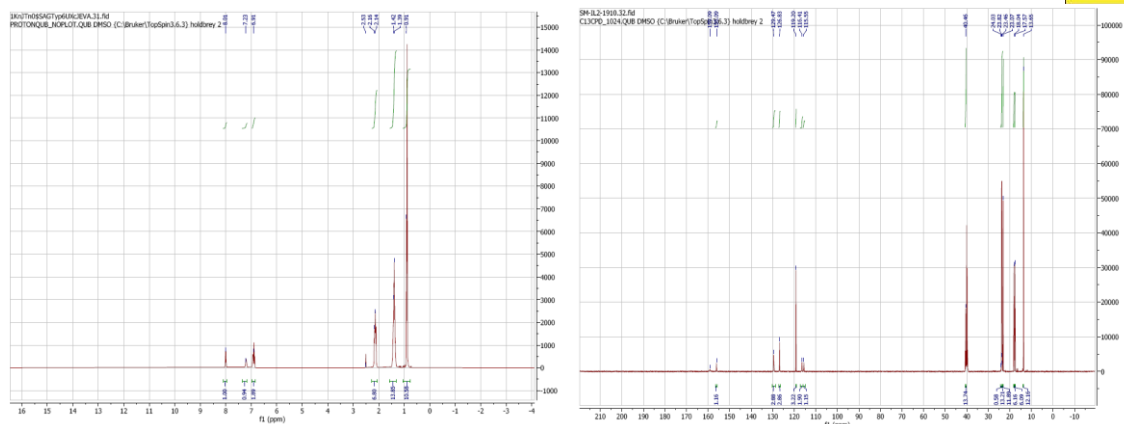


**Figure 2 a** - (left) NMR: (400 MHz, d6-DMSO)  $\delta\text{H}$  = 16.20 (br, 1H, N-H), 11.04 (br, 1H, OH), 7.99 (m, 1H, phenyl ring), 7.42 (m, 1H, phenyl ring), 7.09 (m, 2H, phenyl ring)  
**2 b** - (right)  $\delta\text{C}$  = 155.77 (1C, C-N), 152.12 (1C, phenyl ring), 133.09 (1C, phenyl ring), 129.51 (1C, phenyl ring), 120.18 (1C, phenyl ring), 116.83 (1C, phenyl ring), 110.98 (1C, phenyl ring).

- Having successfully made the substituted tetrazole, the next attempt was to prepare the ionic liquid tetrabutylphosphonium 5-(2-hydroxyphenyl) tetrazolate from tetrabutylphosphonium hydroxide and 5-(2-hydroxyphenyl) tetrazole, to test its LCST behaviour. The prepared ionic liquid  $[\text{P}_{444}][2\text{-OH-Ph-tet}]$  was characterised using  $^1\text{H}$  NMR,  $^{13}\text{C}$  NMR and  $^{31}\text{P}$  NMR spectroscopy to give prominent peaks (Figure 3 a, b, c).

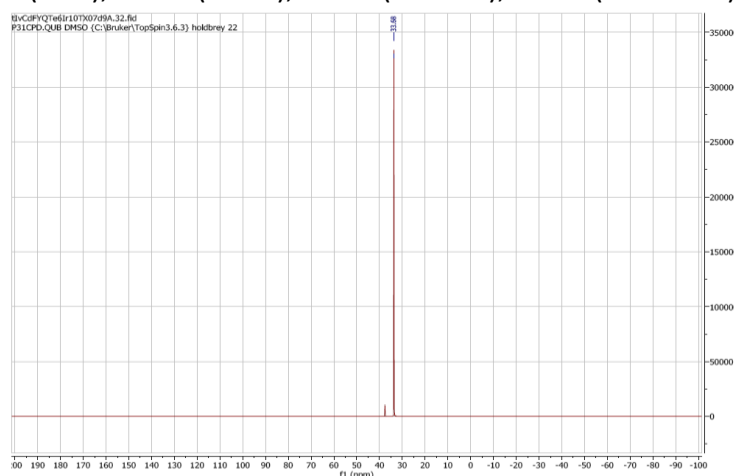






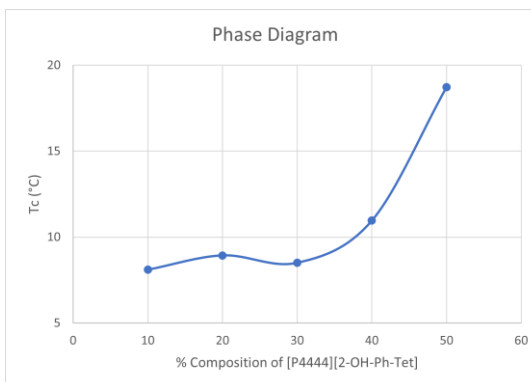
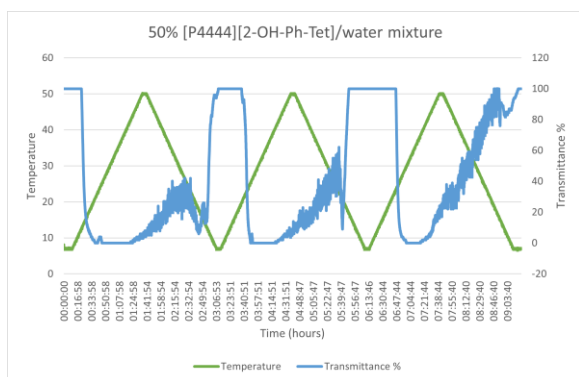
**Figure 3 a** (left) - NMR: (400 MHz, d<sub>6</sub>-DMSO)  $\delta$ H = 8.01 (m, 1H, phenyl ring), 7.23 (m, 1H, phenyl ring), 6.91 (m, 2H, phenyl ring), 2.16 (m, 8H, P-(CH<sub>2</sub>)<sub>4</sub>), 1.42 (m, 16H, P-(C-CH<sub>2</sub>)<sub>4</sub>, P-(C-CH<sub>2</sub>)<sub>4</sub>), 0.91 (m, 12H, P-(C-C-C-CH<sub>3</sub>)<sub>4</sub>)

**3 b** (right) -  $\delta$ C = 159.09 (1C, C-N), 156.09 (1C, C-O), 129.47 (1C, phenyl ring), 126.83 (1C, phenyl ring), 119.20 (1C, phenyl ring), 116.41 (1C, phenyl ring), 115.55 (1C, phenyl ring), 23.82 (P-C-), 23.07 (P-C-C), 18.04 (P-C-C-C), 13.65 (P-C-C-C-C)



**Figure 3 c** - <sup>31</sup>P NMR: [P<sub>4444</sub>][2-OH-Ph-tet]  $\delta$  31P(DMSO-d<sub>6</sub>): 33.68 (P-CH<sub>2</sub>-CH<sub>2</sub>-CH<sub>2</sub>-CH<sub>3</sub>).


5. Having formed the ionic liquid, its cloud point temperature for a few compositions (10%,20%,30%,40%,50%) were determined by using Crystal 16 analyser (Figures 4 a, b and c).



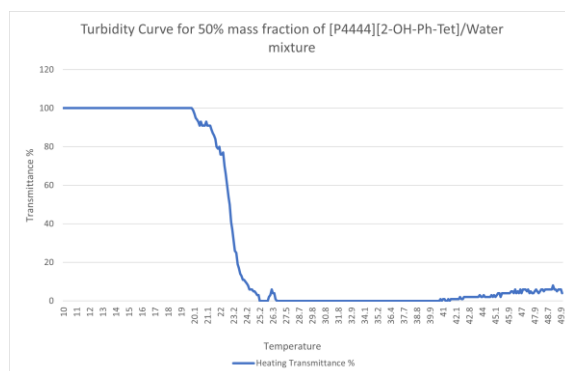


**Figure:4 a (top left) and 4c (bottom) - Turbidity Curves for 50% composition of the ionic liquid.**  
**Figure 4b (top right) - Phase diagram showing relation between critical temperatures versus 10 to 50% composition.**

6. Preparation of a poster for the ILMAT-6 Conference to be held in France from 22<sup>nd</sup> to 26<sup>th</sup> November 2021.

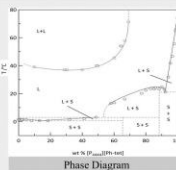
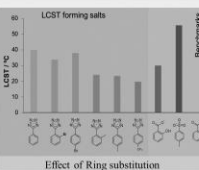

**6<sup>th</sup> International Conference on Ionic Liquid-based Materials**  
 November 22-26, 2021  
 Obernai, France

## LCST behaviour of functionalised tetrabutylphosphonium phenyl-tetrazolate/aqueous mixtures


Sanskriti MADHUKAILYA,\* Junzhe QUAN, Joshua O'HAGAN, Marijana BLESIC, Leila MOURA, and John D HOLBREY  
 The QUILL Research Centre, Queen's University Belfast, Belfast UK

### Abstract

- Tetrabutylphosphonium 5-phenyl tetrazolate ([P<sub>4444</sub>][Ph-Tet]) has LCST behaviour in water with a critical temperature of ~40 °C [2].
- We have ongoing interest in how to control both critical temperatures and phase compositions at LCST point by modifying the phenyl ring of the anion.
- This requires (i) optimization of synthesis for generating tetrazole precursors, and (ii) improved, rapid screening to measure the LCST cloud points.


### Why is it important?



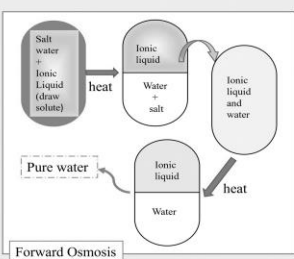
United Nations Sustainable Development Goals: 1 in 3 people do not have access to safe drinking water

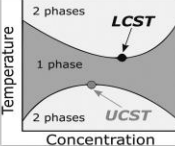
> Separation membrane technology as one of the promising methods for water treatment.

- Pressure-driven membrane process (PDMP),
- Osmosis-driven membrane process (ODMP).



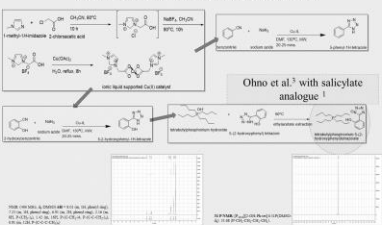
Source: Wikipedia, Wikipedia





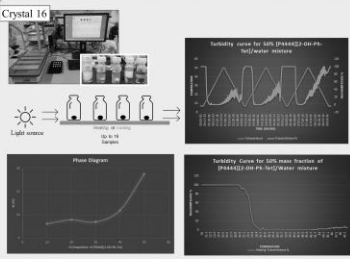
### Synthesis

Preparation of the tetrazoles, the corresponding ionic liquid and further checking the cloud point temperature (LCST)



\* Ohno et al.<sup>3</sup> with salicylate analogue!

### Screening







### Acknowledgement

Professor John Holbrey  
 Dr Leila Moura  
 Dr Joshua O'Hagan  
 Dr Timea Blesic  
 Dr Marijana Blesic  
 Dr Leila Moura  
 Queen's University Belfast

### Reference

1. B. C. Bolintineanu et al., *Chemical Science*, 2015, 6, 105-107.
2. M. M. M. et al., *Chemical Science*, 2017, 8(2), 1161-1169.
3. T. Bolintineanu et al., *Chem. Commun.*, 2015, 14, 1060-1070.
4. T. Bolintineanu et al., *Chem. Commun.*, 2015, 14, 1060-1070.
5. W. W. et al., *Chemical Science*, 2015, 6, 1145-1155.
6. W. W. et al., *Chemical Science*, 2015, 6, 1145-1155.
7. C. Y. et al., *Chem. Commun.*, 2015, 14, 1060-1070.
8. J. Bolintineanu et al., *Chem. Commun.*, 2015, 14, 1060-1070.
9. R. D. Padgett et al., *Acc. Chem. Res.*, 2010, 43, 1197-1217.

Sanskriti Madhukailya, jmadhukailya@qub.ac.uk



## QUILL Quarterly Report

August 2021 – October 2021

<b>Name:</b>	David McAreavey		
<b>Supervisor(s):</b>	Dr Stephen Glover, Dr Oana Istrate and Prof Peter Nockemann		
<b>Position:</b>	PhD Student		
<b>Start date:</b>	1 <sup>st</sup> October 2021	<b>Anticipated end date:</b>	31 <sup>st</sup> March 2025
<b>Funding body:</b>	Department for the Economy		

### Design and Development of an Effective and Interconnected Smart Fire Suppression System for Lithium-ion Batteries in Electric Vehicles

#### Project progress

At this early stage of the project, most progress has taken the form of literature review and developing a rounded knowledge of the current state of technology. This encompasses looking at the direction of the electric vehicle industry, trends reviewed include the transition in the electric vehicle market from the established skateboard configuration of pack design, towards the integration of “cell to pack” and “cell to car” designs. In these designs the cells are multifunctional, carrying mechanical loads as well as storing energy. Additionally, manufacturers are targeting lower part counts and simplification of their electrified products. This has significant implications for systems that aim to suppress or mitigate thermal events, such that the space within the packs is being greatly reduced as well as increasing module sizes.

Surprisingly, despite the number of large OEMs working on structural packs and multifunctional design, there is not yet a consensus on the most appropriate cell form factor to use, with quite a wide spread of manufacturers across the main three cell types. Iron phosphate cells are also becoming more prominent in entry level vehicles, as manufacturers try to reduce their dependence on certain precious materials like nickel. There are still a number of manufacturers that use pouch cells that don’t currently have any obvious way of incorporating multifunctional design into their packs, due to the relatively weak structure of these cells. Additionally, the swelling of these cells in use means that they are difficult to embed in laminates as research has shown, this swelling results in the cells detaching from the laminate and not transferring load, making structural packs with pouch cells ineffective.

There are a range of options for lithium-ion fire suppression and containment on the market, but the high variability of the cell chemistry, size, experimental set up, suppression initiation, spray pattern and pressure used in the case of liquid suppressants, makes the process of comparing different studies quite challenging. These systems need to find an effective balance between the cooling rate required to prevent neighbouring cells heating to the point of reaching thermal runaway, while also suppressing the combustion of any cell that has already ignited.

There are additional questions to be asked about the potential for more thermal runaway events as cells state of health degrade over time. The EV market has not yet seen the effect of high numbers of EVs on the roads with battery packs that have endured hundreds of thousands of miles. This will change as the regulations force the general public to more seriously consider electrified options for their next car. The degradation rate of the cells inside electrified vehicles is only starting to be seen



at scale in the second-hand market, and their state of health has shown a high dependence on the design choices made in the cooling system as well as the way in which the vehicle is used by its owner. Frequent fast charging along with charging to maximum capacity regularly has proven damaging over extended periods.

The continual development of the production processes that cell manufacturers are using also shows hope for improvements in incident rates that come from manufacturing defects. Technology like laser cutting of tabs will reduce the likelihood of burs for example.

### **Future direction of the project**

With the project in its infancy the direction will likely shift with time, at present the next steps envisaged will include evaluating the trade-off between early detection of a system fault, and magnitude of the corrective action. This should allow the development of a system that has the ability to terminate thermal runaway before it takes hold of a cell array, and the corrective action that would be required by a system would be too significant that it is impractical to be fitted internally on a vehicle.

Additionally there is a limit to the knowledge of how to model different types of cell failure initiation, investigating this further may allow improved modelling that can be used to predict the propagation of failure more accurately.

## QUILL Quarterly Report

August 2021 – October 2021

<b>Name:</b>	Sam McCalmont		
<b>Supervisor(s):</b>	Dr Leila Moura, Prof John Holbrey and Prof Margarida Costa Gomes		
<b>Position:</b>	PhD		
<b>Start date:</b>	Jan 2020	<b>Anticipated end date:</b>	2023
<b>Funding body:</b>	EPSRC Doctoral Training Partnership		

### Chemisorbent materials for olefin and paraffin separation

#### Objective of this work

Develop and test new chemisorbent materials for the separation of light olefins and paraffins. In this, achieving high capacity and selectivity for the selected materials. To test this, equipment will be installed, commissioned, and benchmarked for testing under approximate industrial gas stream compositions.

#### Progress to date

Since the last report, ethyl-ammonium nitrate, (butyl-4-cyanopyridinium bis(trifluoromethylsulfonyl)imide and butyl-3-cyanopyridinium bis(trifluoromethylsulfonyl)imide) have been synthesised for testing the solubility of ethylene and ethane. The ethyl-ammonium nitrate proposed by Prof. Margarida Costa Gomes and the cyanopyridinium ionic liquids suggested by Nimal Gunaratne. These molecules shown in Figure 1.

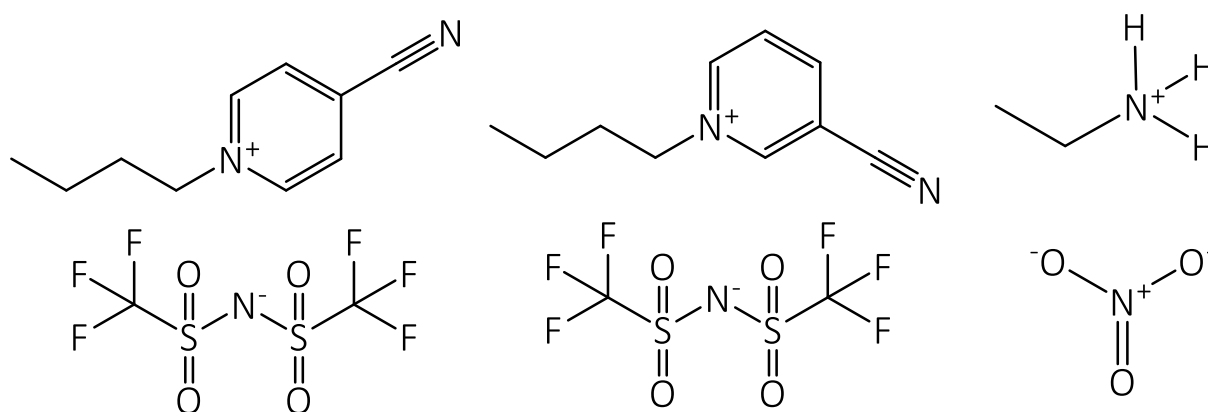


**Figure 1** - Butyl-4-cyanopyridinium bis(trifluoromethylsulfonyl)imide (left) and butyl-3-cyanopyridinium bis(trifluoromethylsulfonyl)imide (middle) and ethyl-ammonium nitrate (right).

The gas solubility system (GSS) was being upgraded to remove the equilibrium chamber in place of a reactor. This reactor would allow for *in-situ* monitoring of the temperature of the ionic liquid. This was a limitation of the previous set up as the equilibrium chamber was heated with no internal monitoring of the ionic liquid temperature. The introduction of the reactor required calibrating the system again as the volume of the headspace has changed. This is done by the gas expansion method as done previously for the equilibrium chamber.



From September, it was planned for a conference at the end of November 2021 to see the influence of the cyanopyridinium ionic liquids have on the solubility of ethylene and ethane, because it has previously been shown that cyanopyridinium ionic liquids formed charge transfer complexes with naphthalene. These tests include high pressure NMR (to see any interactions between the hydrocarbons and cyanopyridinium ionic liquids), the screening method (the screening method allowing for initial solubility tests to be conducted), and the solubility of the hydrocarbons in the gas solubility system.

## References

1. C. Hardacre, J. D. Holbrey, C. L. Mullan, M. Nieuwenhuyzen, T. G. A. Youngs, D. T. Bowron and S. J. Teat, *Phys. Chem. Chem. Phys.*, 2010, **12**, 1842–1853.

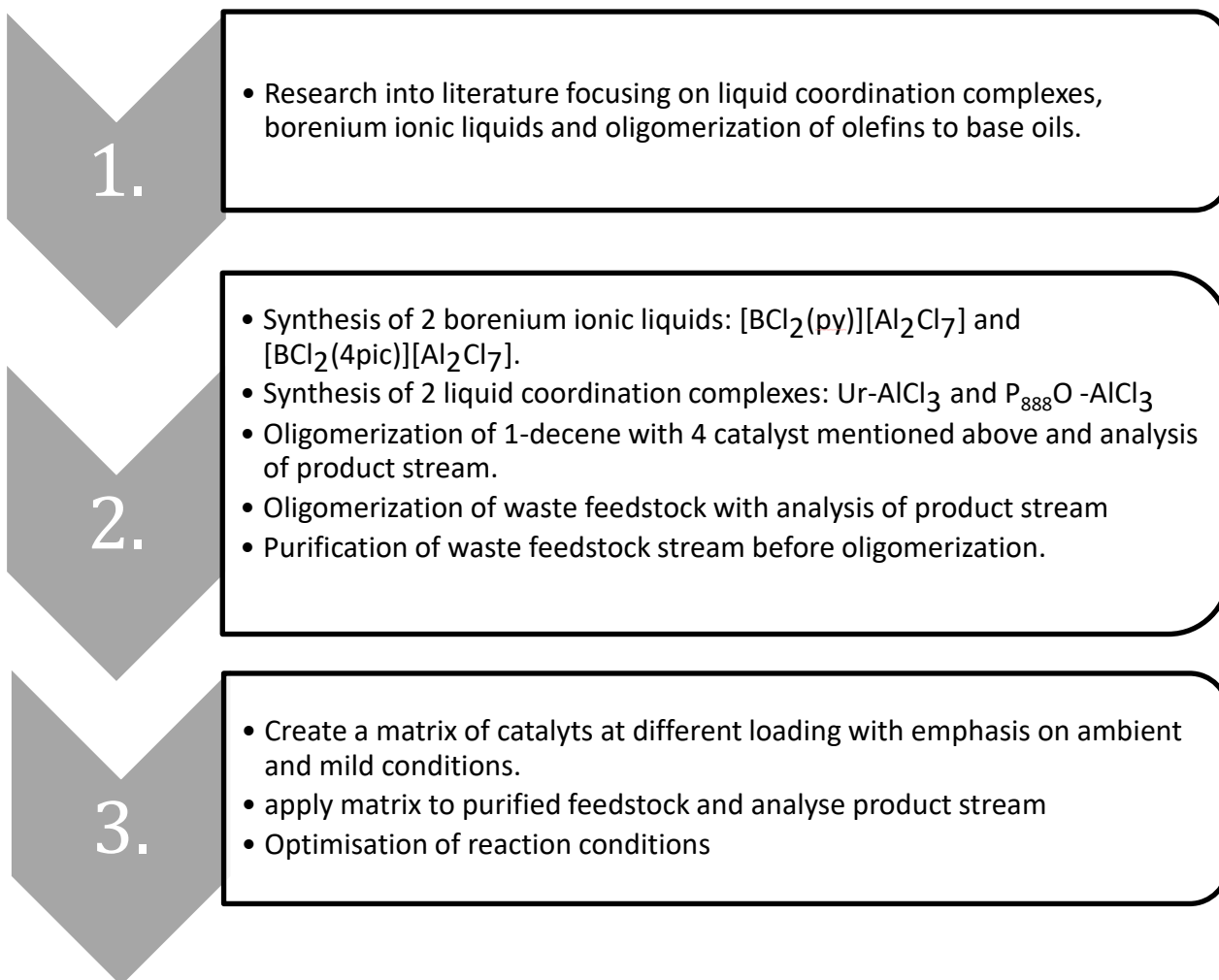
## QUILL Quarterly Report

August 2021 – October 2021

<b>Name:</b>	Emma McCrea		
<b>Supervisor(s):</b>	Prof Gosia Swadzba-Kwasny and Prof John Holbrey		
<b>Position:</b>	PhD student		
<b>Start date:</b>	1/10/21	<b>Anticipated end date:</b>	30/9/24
<b>Funding body:</b>	EPSRC		

### Acidic Ionic Liquids As Catalysts For The Valorisation Of Waste Plastic Resource

In this project, the chemical recycling of waste plastic feedstock will be investigated with the use of liquid coordination complexes and ionic liquids as Lewis acid catalysts. The aim is to develop an inexpensive acidic ionic liquid catalyst that can function with highly contaminated feedstocks. The oligomerisation of olefins will transform the feedstock into lubricating base oil which is used in a range automotive machine to improve efficiency.



## QUILL Quarterly Report

August 2021 – October 2021

<b>Name:</b>	Anne McGrogan		
<b>Supervisor(s):</b>	Prof Gosia Swadzba-Kwasny		
<b>Position:</b>	PhD		
<b>Start date:</b>	01/10/2019	<b>Anticipated end date:</b>	31/03/2023
<b>Funding body:</b>	EPSRC		

### Boron Lewis acids: structure and applications

#### Background: Boron Lewis acids as co-catalysts for nitrogen activation

I have previously synthesised a wide range of boron compounds and I will explore the use of these boron Lewis acids as co-catalysts for nitrogen activation. Nitrogen is an essential element for all living things; it has a key role in proteins and nucleic acids, providing the nitrogen content needed to create plants, animals, and other organisms. Biological nitrogen activation by nitrogenase enzymes operates under ambient conditions by employing transition metal-based active sites to bind and reduce the dinitrogen molecule, subsequently releasing it as  $\text{NH}_3$  or  $\text{NH}_4^+$ . While the currently used industrial process requires elevated temperatures and pressures ( $\sim 500^\circ\text{C}$  and  $>100$  atm), to combine  $\text{N}_2$  and  $\text{H}_2$ , over an Fe-based catalyst.<sup>1,2</sup> These forcing conditions are required due to the high energy barrier for  $\text{N}_2$  triple bond cleavage. The energy requirement to produce  $\text{NH}_3$  for fertilisers in the Haber–Bosch process is estimated to be approximately 1.5% of the annual global energy supply.<sup>3</sup> Therefore, more sustainable methods for ammonia synthesis, with reduced energy consumption are desirable.

#### 1.1 Introduction to homogenous $\text{N}_2$ activation by $\text{Fe}^0$ -based catalysts

The presence of iron in both industrial and biological systems, has led to it being the metal of interest in many dinitrogen activation studies. Even though,  $\text{N}_2$  is a poor  $\sigma$ -donor and  $\pi$ - acceptor, many Fe- $\text{N}_2$  complexes have been synthesised with a variety of ligands.<sup>1</sup> The extent of activation of the coordinated  $\text{N}_2$  ligand is commonly measured by examining the N-N bond lengths and N–N stretching frequency by IR or Raman spectroscopy.

In 2013, Peters *et al.*<sup>4</sup> reported on several Fe catalysts for the conversion of  $\text{N}_2$  to  $\text{NH}_3$ . They found that catalytic yields of approximately 7 equiv. of  $\text{NH}_3$  per Fe could be formed in diethyl ether at  $-78^\circ\text{C}$  using the acid  $\text{H}(\text{BAr}^{\text{F}})_4$  (46 equiv.) and the very strong reductant  $\text{KC}_8$  (50 equiv.) as the proton and electron sources, respectively. In 2017, they reported a significant improvement in yield (80 equiv.  $\text{NH}_3$  per Fe) when a significantly weaker combination of reductant ( $\text{Cp}^*_2\text{Co}$ ) and acid ( $[\text{Ph}_2\text{NH}_2][\text{OTf}]$ ) was used (Figure 1).<sup>5</sup>

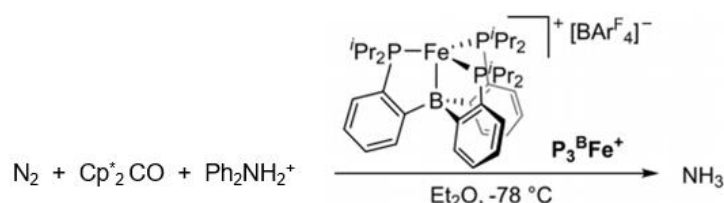


**Figure 1** - Summary of the catalytic conversion of  $\text{N}_2$  to  $\text{NH}_3$  by  $\text{P}_3\text{BFe}^+$  and the conditions used.



Szymczak et al.<sup>6</sup> reported an alternative N<sub>2</sub> activation strategy that is shown to weaken the N-N bond and enhance protonation selectivity through the simple addition of Lewis acids to an Fe(0)-N<sub>2</sub> unit. The idea was to test the “push-pull” hypothesis by which electron density is “pushed” from a reduced iron centre and “pulled” into the N<sub>2</sub> unit by adjacent Lewis acidic sites, thus rendering it more reactive towards protonation. They investigated adducts formed between the iron-dinitrogen complex, [Fe(depe)<sub>2</sub>(N<sub>2</sub>)] (depe=1,2-bis(diethylphosphino)ethane) and several Lewis acids such as B(C<sub>6</sub>F<sub>5</sub>)<sub>3</sub> (Figure ). From their studies, they reported that the N-N bond strength and N<sub>2</sub> binding affinity can be dramatically tuned by the strength of Lewis acidity, quantified by the acceptor number (AN) (Figure ).

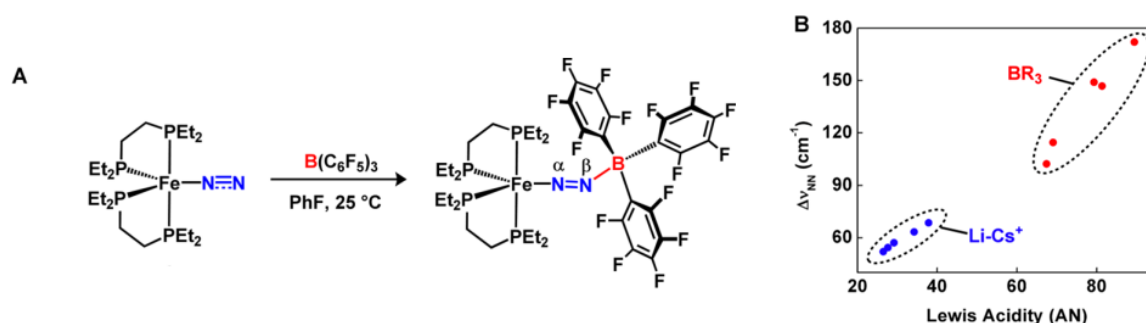


**Figure 2** - (A) Formation of adduct between [Fe(depe)<sub>2</sub>(N<sub>2</sub>)] and B(C<sub>6</sub>F<sub>5</sub>)<sub>3</sub>. (B) Relationship between Lewis acidity and ν<sub>NN</sub> using a variety of Lewis acids (Li<sup>+</sup>, Na<sup>+</sup>, K<sup>+</sup>, Rb<sup>+</sup>, Cs<sup>+</sup>; BR<sub>3</sub> (R = 2,6-F<sub>2</sub>Ph, 2,4,6-F<sub>3</sub>Ph, C<sub>6</sub>F<sub>5</sub>, OC<sub>6</sub>F<sub>5</sub>, F)).<sup>6</sup>

## Progress to date

### Experimental

All manipulations were performed under an atmosphere of dry N<sub>2</sub> using standard Schlenk line techniques, or in an MBraun Labmaster DP glovebox. All glassware was dried at 170 °C overnight before use. Chemicals were obtained from Sigma-Aldrich and used without further purification. Solvents were dried over 3 Å molecular sieves. THF-d<sub>8</sub> was freeze-pump-thaw degassed and dried over 3 Å molecular sieves.

Ongoing synthesis of Fe(depe)<sub>2</sub>Cl<sub>2</sub>: A solution of depe (0.5 g, 0.00333 mmol) was prepared in 50 mL of DCM and added dropwise to a slurry of FeCl<sub>2</sub> (0.2 g, 0.00167 mmol) in 100 mL DCM in the glovebox and stirred overnight. Solvent was removed *in vacuo*. Awaiting analysis.

### Structural studies of boron compounds

Transition metals are widely recognised for their ability to function as good catalysts, but they have major drawbacks such as low abundance, high cost and toxicity. Boron is a main group, non-metallic, earth-abundant element with the potential to replace transition metals.<sup>1</sup> Many boron-based species show very strong Lewis acidity (*i.e.* excellent electron-pair acceptors).<sup>2</sup> However, understanding, quantifying and predicting Lewis acidity is very challenging, which limits the development of boron-based catalysts. Usually, measurement of Lewis acidity is probe-dependent, therefore order of strength on Lewis acidity scale may vary, depending on the probe used and the methodology adopted. In addition, there are limited experimental measurements of electronic structure of boron compounds. A major challenge for obtaining experimental electronic structure data is the presence of the boron centre. The boron 1s core orbital has an energy of ~200 eV, meaning that vacuum conditions are required for any electronic structure measurements. I am currently working on a study which will utilise liquid-microjet x-ray spectroscopy using the soft x-ray synchrotron BESSY II, Berlin, to determine the valence electronic structure of boron-containing samples. This research will



be done in collaboration with Dr Kevin Lovelock from the University of Reading, who will be analysing the results. The aim is to use this data to better quantify, understand, and predict the Lewis acidity of boron-based species. By understanding how the electronic structure relates to chemical reactivity, it will help aid the design of new boron based catalytic systems. To achieve this goal a combination of liquid-jet sample delivery with x-ray photoelectron spectroscopy (XPS), resonant XPS (RXPS) and x-ray absorption spectroscopy (XAS) will be used to study a range of boron-containing samples. These include reference samples and a selection of 3 and 4 coordinate boron-based species with formal charges -1, 0, +1. Suggested samples are shown in Table 1.

Boron 1s XPS, along with calculations, will be used to probe the atomic charge of the boron centres; this is important for understanding and predicting reactivity. The atomic charge for ligands bonded to boron will also be probed (O 1s, Cl 2p, P 2p).

RXPS is a site-specific technique involving resonant core level excitation followed by de-excitation through Auger electron emission. The boron-based molecular orbitals (MO) for all compounds are expected to be at a similar binding energy to solvent MOs. Using standard XPS, identification of boron-based solute MOs would be very difficult due to how they are swamped by signal from solvent MOs. RXPS of B 1s will allow identification of these boron-based MOs. Furthermore, RXPS will allow identification of MOs from ligands bonded to boron (O 1s, Cl 2p, P 2p).

B 1s XAS will be recorded using partial Auger yield detection (as part of the RXPS measurements). XAS, along with time-dependent DFT calculations, will be used to identify the boron-based unoccupied MOs. In addition, unoccupied MOs for ligands bonded to boron will be identified (O 1s, Cl 2p, P 2p).

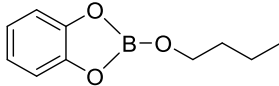
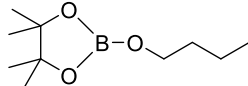
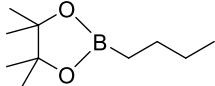
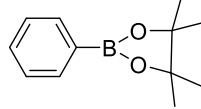
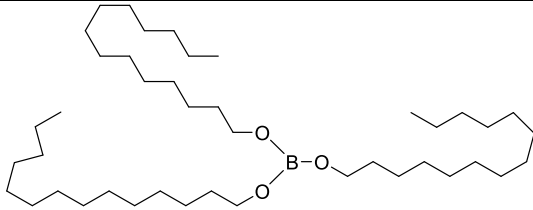
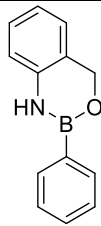
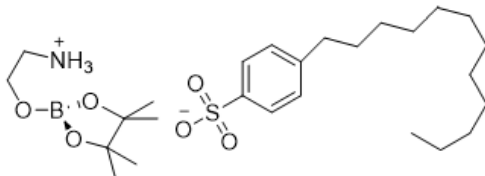
### *2.1 Objective of this work*

The aim is to gain a better understanding of how the electronic structure of boron-based species relate to chemical reactivity which will help aid the design of new boron based catalytic systems.

### *2.2 Progress to date*

Finalising the sample set of boron compounds to be tested at BESSY II in December. Table 1 shows some of the compounds that will be tested.

**Table 1** - Charge-neutral tricoordinate boron compounds synthesised in this work.

Compound code name	Structure	Compound code name	Structure
B(cat)(OBu)		B(pin)(OBu)	
B(pin)(Bu)		PhB(pin)	
B(OC <sub>14</sub> ) <sub>3</sub>		PhB(C <sub>7</sub> H <sub>9</sub> NO)	
[B(pin)(MEA)] [C <sub>12</sub> LAB]			

#### Synthesis of [P<sub>66614</sub>][BOB] and [P<sub>66614</sub>][BH<sub>4</sub>]

The ionic liquids, trihexyl(tetradecyl)phosphonium bis(oxalato)borate, [P<sub>66614</sub>][BOB] and trihexyl(tetradecyl)phosphonium borohydride, [P<sub>66614</sub>][BH<sub>4</sub>] were synthesised as a part of a collaboration project between QUILL and the University of Silesia in Katowice. The aim of the project is to investigate first-order liquid-liquid transitions (LLT) in a series of ionic liquids containing trihexyl(tetradecyl)phosphonium cation [P<sub>666,14</sub>]<sup>+</sup> and anions of different sizes and shapes, providing an insight into the structure-property relationships governing LLT.

### Experimental

#### Synthesis of sodium bis(oxalato)borate, Na[BOB]

Oxalic acid (0.03 mol eq.) and boric acid (0.01 mol eq.) were separately dissolved in water and then mixed together under constant stirring. Na<sub>2</sub>CO<sub>3</sub> (0.5 mol eq.) was slowly added to the mixture with vigorous stirring. The turbid solution was heated in an oil bath at 120 °C and the water collected by distillation until a dry white powder was obtained. The crude product was dispersed in hot acetonitrile at 60 °C and stirred for one more hour. Then a white powder was isolated using vacuum filtration. The product was further washed with cold ethanol and the powder was dried under high vacuum (overnight, 60 °C, 10<sup>-2</sup> mbar). <sup>1</sup>H, <sup>13</sup>C, <sup>11</sup>B NMR spectra were recorded in CDCl<sub>3</sub>.

#### Synthesis of trihexyl(tetradecyl)phosphonium bis(oxalato)borate, [P<sub>66614</sub>][BOB]

Trihexyl(tetradecyl)phosphonium chloride [P<sub>66614</sub>]<sup>+</sup>Cl<sup>-</sup> (0.010 mol eq.) and sodium bis(oxalato)borate (0.010 mol eq.) were mixed in 150 ml of dichloromethane. The reaction mixture was stirred overnight at room temperature and then water was added under continuous stirring. The aqueous layer was separated, and the organic layer was collected and washed with deionised water (100 cm<sup>3</sup>). Subsequent washes were performed with solution of Na[BOB] in deionised water. Final three washes were performed with deionised water until no chloride could be detected with silver nitrate solution. Subsequently, DCM was removed *via* rotary evaporation (30 min, 35 °C) and the ionic liquid was dried under high vacuum (overnight, 60 °C, 10<sup>-2</sup> mbar).



<sup>2</sup> mbar). <sup>1</sup>H, <sup>13</sup>C and <sup>31</sup>P NMR spectra were recorded in CDCl<sub>3</sub>. XRF analysis confirmed chloride content was below the detectable limit.

*Synthesis of trihexyl(tetradecyl)phosphonium borohydride, [P<sub>66614</sub>][BH<sub>4</sub>]*

Trihexyl(tetradecyl)phosphonium chloride [P<sub>666,14</sub>]Cl (0.010 mol eq.) and sodium borohydride, Na[BH<sub>4</sub>] (0.013 mol eq.) were separately added to 25 cm<sup>3</sup> deionised water (total 50 cm<sup>3</sup>) and then combined in a round-bottomed flask (250 cm<sup>3</sup>), resulting in the formation of a biphasic liquid system; the mixture was left to react (1 h, room temperature, 600 rpm). The aqueous layer was separated, and the organic layer was collected and washed, firstly with deionised water (10 cm<sup>3</sup>) and then dichloromethane, DCM (10 cm<sup>3</sup>). Subsequent washes were performed with solution of Na[BH<sub>4</sub>] in deionised water. Final three washes were performed with deionised water until no chloride could be detected with silver nitrate solution. Subsequently, DCM was removed *via* rotary evaporation (30 min, 35 °C) and the ionic liquid was dried under high vacuum (overnight, 70 °C, 10<sup>-2</sup> mbar). <sup>1</sup>H, <sup>13</sup>C, <sup>11</sup>B and <sup>31</sup>P NMR spectra were recorded in *d*<sub>6</sub>-DMSO solution. XRF analysis confirmed chloride content was below the detectable limit.

## References

1. J. L. Crossland and D. R. Tyler, *Coord. Chem. Rev.*, 2010, **254**, 1883–1894.
2. G. P. Connor and P. L. Holland, *Catal. Today*, 2017, **286**, 21–40.
3. L. Wang, M. Xia, H. Wang, K. Huang, C. Qian, C. T. Maravelias and G. A. Ozin, *Joule*, 2018, **2**, 1055–1074.
4. J. S. Anderson, J. Rittle and J. C. Peters, *Nature*, 2013, **501**, 84–87.
5. M. J. Chalkley, T. J. Del Castillo, B. D. Matson, J. P. Roddy and J. C. Peters, *ACS Cent. Sci.*, 2017, **3**, 217–223.
6. J. B. Geri, J. P. Shanahan and N. K. Szymczak, *J. Am. Chem. Soc.*, 2017, **139**, 5952–5956.

## QUILL Quarterly Report

August 2021 – October 2021

<b>Name:</b>	Shannon McLaughlin		
<b>Supervisor(s):</b>	Prof Gosia Swadźba-Kwaśny		
<b>Position:</b>	PhD Student (2 <sup>nd</sup> year)		
<b>Start date:</b>	October 2020	<b>Anticipated end date:</b>	July 2024
<b>Funding body:</b>	Department for the Economy		

### Pressure-induced liquid-liquid transition in a family of ionic materials

#### Introduction

The phase transitions usually studied tend to occur between a solid phase and a liquid phase, these include crystallisation and glass transitions. Liquids can also exist in different states and can exhibit polymorphism. Liquid polymorphism is when there are two or more liquid states existing for a single component material. A transformation from one of these liquid states to another is known as a liquid-liquid transition or LLT. Only four molecular liquids have been found with evidence for LLTs. These are water, triphenyl phosphate, n-butanol, and D-mannitol. In this work, a first-order liquid-liquid transition has been reported in a series of ionic liquids for the first time. The seven ionic liquids chosen for this study all contained the trihexyl(tetradecyl)phosphonium ( $[P_{66614}]^+$ ) cation along with a combination of various anions. The phosphonium cation was selected as it provides the ionic liquids with ionic conductivity as well as relatively high thermal and electrochemical stabilities. The various anions were selected due to their differences in size, geometry, conformational and coordinating ability.  $[SCN]^-$ ,  $[TCM]^-$  and  $[BF_4]^-$  anions are all rigid due to their small size. Comparatively, the  $[BOB]^-$  anion is much bulkier but is still rigid due to the distorted tetrahedral geometry around the central boron atom. The  $[TFSI]^-$  anion has both *cis* and *trans* conformers and the  $[TAU]^-$  anion features a flexible alkyl chain allowing for multiple conformations. The range of different sizes and shapes of the anions helps to provide an insight into the structure-property relationships governing LLT. The structure of the various anions are illustrated in figure 1. The donor numbers of these anions are also shown which provides information regarding their Lewis basicity.

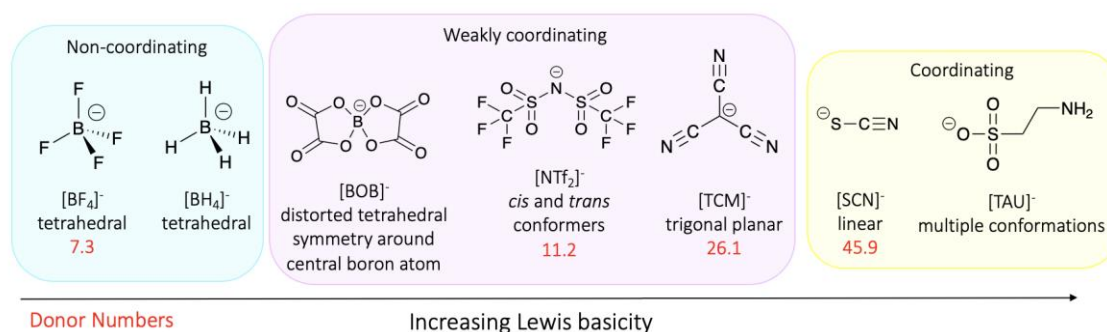
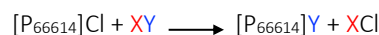
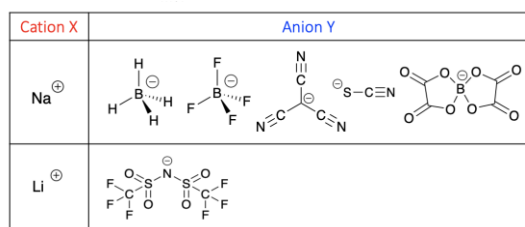


**Figure 1** - Structure of the various anions under investigation in order of increasing Lewis basicity

#### Synthesis of Ionic Liquids

The synthesis of  $[P_{66614}][BF_4]$ ,  $[P_{66614}][NTf_2]$ ,  $[P_{66614}][TCM]$  and  $[P_{66614}][SCN]$  has been described in previous quarterly reports. These ionic liquids were generated by starting from either the sodium or lithium salt. These salts underwent an anion exchange with  $[P_{66614}][Cl]$  to form the corresponding

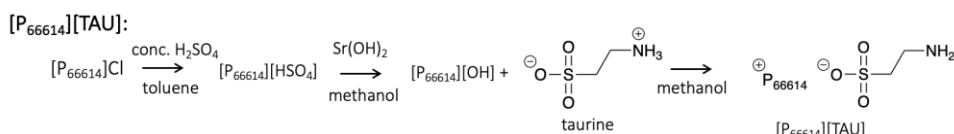
ionic liquids (Scheme 1). Multiple washes were performed with salt solutions as well as deionised water. XRF analysis was used to confirm the purity of these ionic liquids and ensure the chloride content was below 200 ppm.



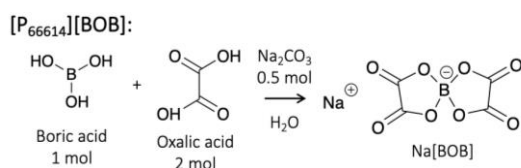
**Scheme 1** - General equation for anion exchange reaction

[P<sub>666,14</sub>][BH<sub>4</sub>]. Trihexyl(tetradecyl)phosphonium chloride [P<sub>666,14</sub>]Cl (0.010 mol eq.) and sodium borohydride, Na[BH<sub>4</sub>] (0.013 mol eq.) were separately added to 25 cm<sup>3</sup> deionised water (total 50 cm<sup>3</sup>) and then combined in a round-bottomed flask (250 cm<sup>3</sup>), resulting in the formation of a biphasic liquid system; the mixture was left to react (1 h, room temperature, 600 rpm). The aqueous layer was separated, and the organic layer was collected and washed, firstly with deionised water (10 cm<sup>3</sup>) and then dichloromethane, DCM (10 cm<sup>3</sup>). Subsequent washes were performed with solution of Na[BF<sub>4</sub>] in deionised water. Final three washes were performed with deionised water until no chloride could be detected with silver nitrate solution. Subsequently, DCM was removed via rotary evaporation (30 min, 35 °C) and the ionic liquid was dried under high vacuum (overnight, 70 °C, 10<sup>-2</sup> mbar). <sup>1</sup>H, <sup>13</sup>C, <sup>11</sup>B and <sup>31</sup>P NMR spectra were recorded in d<sub>6</sub>-DMSO solution. XRF analysis recorded a chloride content of ppm with a lower detection limit (LLD) of .

[P<sub>666,14</sub>][TAU] was on to generate [P<sub>666,14</sub>] hydrogen sulphate and subsequently [P<sub>666,14</sub>] hydroxide. The synthesis of [BOB] involved reacting boric acid with oxalic acid in the presence of sodium carbonate to generate the sodium salt.



**Scheme 2** - Synthesis of [P<sub>666,14</sub>][TAU]



**Scheme 3** - Synthesis of [P<sub>666,14</sub>][BOB]

### Calorimetric studies of phase transitions

These ionic liquids were then used in a collaborative study with the Wojnarowska research group. This involved several temperature and pressure based studies: the first of which being a calorimetric study. DSC thermograms were analysed to confirm the presence of a liquid-liquid transition and show its reversibility without crystallisation.



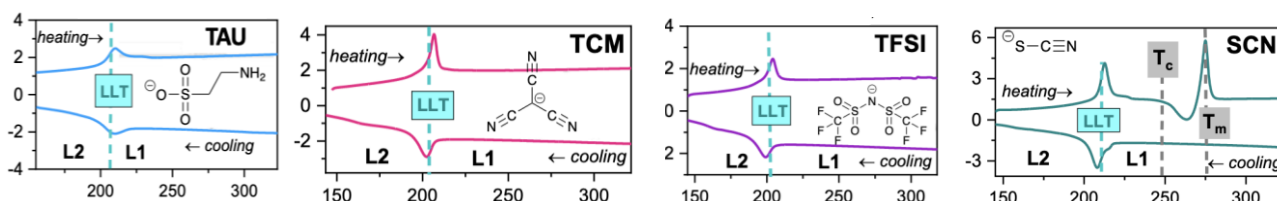


**Figure 2** - DSC thermograms of [P<sub>66614</sub>][TAU], [P<sub>66614</sub>][TCM], [P<sub>66614</sub>][TFSI] and [P<sub>66614</sub>][SCN]

[TAU]<sup>-</sup>, [TCM]<sup>-</sup> and [TFSI]<sup>-</sup> ionic liquids all show a broad exothermic peak when heated and a sharp symmetrical endothermic peak when cooled. The thiocyanate ionic liquid ([SCN]<sup>-</sup>) showed an exothermic peak followed by cold crystallisation. The temperature of the liquid-liquid transition decreases in order; [SCN]<sup>-</sup> < [TAU]<sup>-</sup> < [TCM]<sup>-</sup> < [TFSI]<sup>-</sup>. This corresponds to decreasing basicity and increasing anion size. When the scanning rate was decreased there was no shift in the cooling cycle. This confirmed that a liquid-liquid transition had occurred for these four ionic liquids.

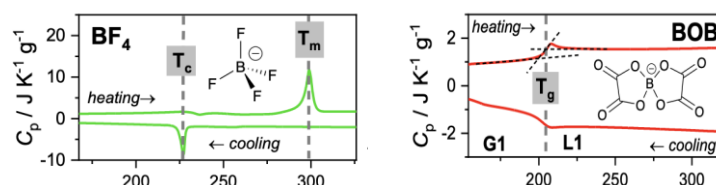


**Figure 3** - DSC thermograms of [P<sub>66614</sub>][BF<sub>4</sub>] and [P<sub>66614</sub>][BOB]

The final two anions displayed different behaviour. From the DSC thermograms in figure 4 you can see that [BF<sub>4</sub>]<sup>-</sup> underwent supercooling to induce crystallisation. Conversely, a step-like transition for was observed for [BOB]<sup>-</sup> agreeing with a vitrification process. In conclusion, large rigid non-coordinating anions such as [BOB]<sup>-</sup> tend to drive vitrification rather than liquid-liquid phase transitions. Large, flexible, asymmetrical anions such as [TFSI]<sup>-</sup> induce liquid-liquid transitions whereas small, symmetrical, non-coordinating anions such as [BF<sub>4</sub>]<sup>-</sup> induce crystallisation. Finally, basic asymmetrical anions such as thiocyanate can feature both liquid-liquid transition and crystallisation behaviour.

### Changes in ion dynamics accompanying LLT

Dielectric spectroscopy was also used to investigate the changes in ion dynamics that occur during a liquid-liquid transition. These changes were measured under both ambient and high-pressure conditions. The  $\beta$  exponent is used to describe the relaxation times in disordered systems.

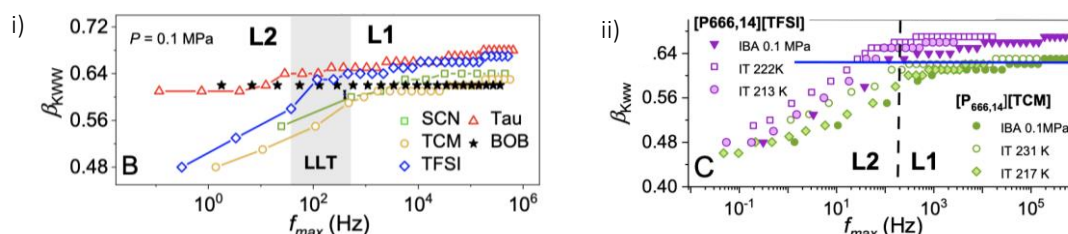


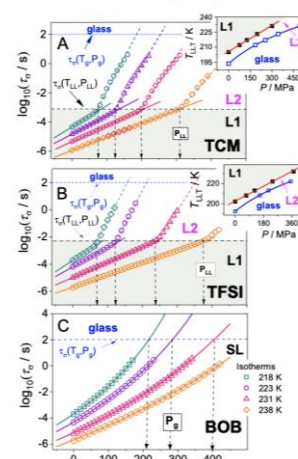
**Figure 4** - Dielectric response of studied ILs measured at i) ambient pressure and ii) high-pressure conditions



In figure 5 i), when moving from liquid 1 to liquid 2 the  $\beta$  exponent decreases for  $[\text{TCM}]^-$ ,  $[\text{TFSI}]^-$ ,  $[\text{SCN}]^-$  and  $[\text{TAU}]^-$ . This indicates that the distribution of relaxation times becomes broader. In liquid 1 the components have similar relaxation times. Whereas in liquid 2 some of the components are more mobile and the relaxation times are not as similar. Corresponding results are observed for  $[\text{TFSI}]^-$  and  $[\text{TCM}]^-$  under high-pressure conditions. Conversely, no change is observed for  $[\text{BOB}]^-$  when going from liquid 1 to liquid 2. This is typical for glass-forming systems and these results agree with the previous calorimetric data.

LLT under high-pressure conditions:

The final part of this research involved the study of ionic liquids under high-pressure conditions. Isothermal compression was used to induce a first order phase transition instead of rapid cooling. Isothermal compression has previously been used to induce liquid-liquid transitions in phosphorus and nitrogen, but it requires extreme temperatures and pressures. The three ionic liquids shown on screen were chosen for high-pressure tests. The graphs represent the pressure dependence of conductivity relaxation time measured at various temperatures. For  $[\text{TFSI}]^-$  and  $[\text{TCM}]^-$  the relaxation times increase at higher pressures. This results in a more disordered phase when moving from liquid 1 to liquid 2. Once again  $[\text{BOB}]^-$  showed no change in relaxation times when moving from liquid 1 to liquid 2. These results once again agree with previous calorimetric and dielectric spectroscopy results.



## Conclusions

In conclusion, a systematic study of  $[\text{P}_{66614}]^+$  based ionic liquids has been conducted. Results confirmed that liquid-liquid transitions were exhibited in four of the ionic liquids under investigation. This study has also helped gain insight into the structure-property relationships governing LLT formation. We have discovered that specific conditions must be met regarding the structure of the anion. These include size, symmetry, flexibility and Lewis basicity.

## Future Work

These will be used in future high-pressure studies. Once we have the results of these additional studies and finalised a few corrections this research paper has been accepted into Nature Communications. Future work will involve applying for neutron scattering studies at ISIS and molecular modelling of samples using Dissolve.

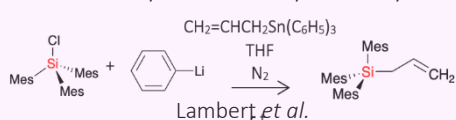
## Synthesis of trimesitylsilane

Future work will involve completing the final two steps of the proposed synthesis of the 'free' trimesitylsilylium cation.

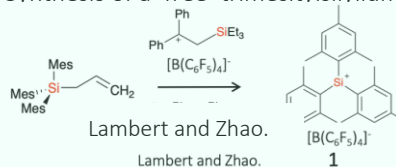
Allyltrimesitylsilane and trimesitylsilylium tetrakis(pentafluorophenyl)borate (compound 1) will be synthesised following methods described by Lambert *et al.* and Lambert and Zhao respectively (Scheme 2 and Scheme 3). After compound 1 has been successfully synthesised, it will be combined with commonly used anions such as  $[\text{NTf}_2]^-$  and  $[\text{FSI}]^-$  to conduct characteristic studies of the cation.



Scheme 2: Synthesis of allyltrimesitylsilane.



Scheme 3: Synthesis of a 'free' trimesitylsilylium cation.



The next aim would be to combine the trimesitylsilylium cation with borate anions or cyanoborate anions (Figure 1) in hope of generating new Lewis superacidic ionic liquids. Applications of these newly developed ionic liquids will then be investigated for potential use as solvents and catalysts.

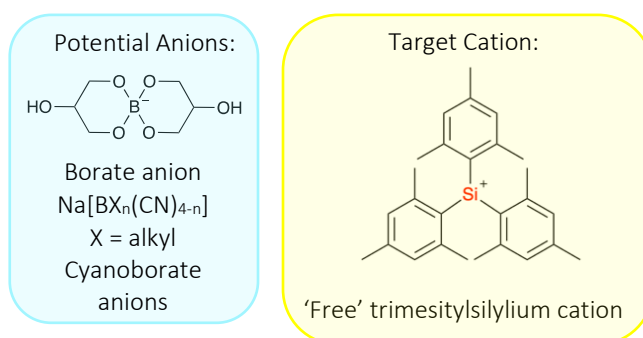


**Figure 5** - Structure of the target trimesitylsilylium cation and potential borate anions or cyanoborate anions



## QUILL Quarterly Report

August 2021 – October 2021

<b>Name:</b>	Hugh O'Connor		
<b>Supervisor(s):</b>	Prof Peter Nockemann, Dr Stephen Glover and Dr Josh Bailey		
<b>Position:</b>	PhD student		
<b>Start date:</b>	October 2019	Anticipated end date:	June 2023
<b>Funding body:</b>	EPSRC/ Shell		

### Redox Flow Battery Materials for Energy Storage

Work has continued developing 3D-printed test cells to improve the performance of Redox Flow Battery design. The next stage of the evolution of the cell design has commenced, scaling the cells up towards commercial scale cells as well as longer term durability testing of cells manufactured *via* 3D-printing. The cells are also being used in QUILL to develop new iron based electrolytes as well as traditional vanadium systems. UV-vis has been used to investigate the SOC of these systems during charge-discharge. Various other avenues for research have also emerged using the 3D-printing platform. These include miniaturised test cells for *operando* study using micro X-ray CT, the use of novel 3D-printing techniques, and development of polypropylene 3D-printing. Other work is also being assisted by a number of undergraduate students, including investigation into graphene nanocomposite membranes, novel cell and stack topologies and a techno-economic evaluation of 3D-printed flow cells.



## QUILL Quarterly Report

August 2021 – October 2021

<b>Name:</b>	Scott Place		
<b>Supervisor(s):</b>	Dr Paul Kavanagh (Primary) and Dr Mark Muldoon (Secondary)		
<b>Position:</b>	PhD Student		
<b>Start date:</b>	Oct 2019	<b>Anticipated end date:</b>	Jul 2022
<b>Funding body:</b>	ESPRC		

### Molecular Electrocatalysts for Energy and Electrosynthetic Applications

Since August, my project has been primarily focused on our TEMPO-Derivative Benchmarking Study, which was mentioned in the previous report. I have been designing a series of experiments using cyclic voltammetry to determine rate constants of a range of organic nitroxide radical oxidation catalysts for use in electro-organic synthesis. This included:

- Studies on appropriate concentration of supporting base (NMI) used in the alcohol oxidation reactions.
- A series of experiments with various concentrations of TEMPO derivatives to confirm first-order activity and appropriate concentration.
- Studies on appropriate concentration of substrate (Benzyl Alcohol).

These experiments were to confirm pseudo-first order conditions, in line with those required for a Saveant Framework for the kinetic analysis of molecular electrocatalysts. Once conditions were established, I was able to estimate rate constants for each of the TEMPO-derivatives for this reaction. This part of the study was highly labour-intensive, requiring a large screening process of 7 different catalysts under a wide range of different conditions.

Once the proper conditions were established, I moved onto larger scale (10 mL) electrolysis experiments. The aim here is to use HPLC or GC to monitor the progress of a reaction and to determine further kinetic information. We hope to see if there is a useful relationship between the data that can be determined from fast cyclic voltammetric studies and the performance of catalysts under real-world synthetic conditions. Presently, I am working with Dr Paul Dingwall's PhD student, Gavin Lennon, on HPLC method development for this particular reaction mixture. I am also working on electrolysis method development. Obtaining reproducible and reliable results can be challenging for this type of study; in real-world synthesis, one would need to be less careful, but for the sake of benchmarking, it is important to keep the method highly consistent between each run.

Within the next week or two, once both above methods have been finalised, I hope to generate a significant amount of data for this study in a relatively short space of time, which I will then use to write a draft for publication, under the guidance of Dr Kavanagh.



## QUILL Quarterly Report

August 2021 – October 2021

<b>Name:</b>	Junzhe Quan		
<b>Supervisor(s):</b>	Prof John Holbrey and Dr Leila Moura		
<b>Position:</b>	PhD		
<b>Start date:</b>	01/10/2019	<b>Anticipated end date:</b>	01/10/2023
<b>Funding body:</b>	Self funding		

### **Use ionic liquids that exhibit LCST (lower critical solution temperature) behaviour as draw fluids for water treatment, desalination and separation**

#### **Background**

New Ionic liquid materials have been recently developed that exhibit lower critical solubility temperature (LCST) behaviour with water, that is, they are miscible at a low temperature and split into two aqueous phases on heating beyond a critical temperature. Such materials have the potential to be used as draw fluids for forward osmosis (FO) water desalination using low grade energy to address the global challenge to provide clean, accessible drinking water to all the world's populations. In this research programme, new ionic liquids will be investigated as advanced fluids for forward osmosis water treatment. This offers opportunities to advance less energy intensive alternative to conventional reverse osmosis as a solution to the global challenge of providing potable water in regions of low availability.

#### **Objective of this work**

My research program in the use of ionic liquids as potential draw fluids for FO water treatment includes:

Preparation of appropriate model ionic liquids

Characterisation of aqueous/ionic liquid phase behaviour as a function of aqueous component salinity, pH, temperature and to draw structure-performance relationships with the ionic liquid cation/anion components.

Develop and validate an automated screening approach to determination of liquid/liquid critical phase behaviour through cloud-point determination

Optimize ionic liquid to use as draw fluid, developing a proof-of-concept ionic liquid-based RO desalination demonstrator for benchmarking

Measure the energy consumption and compare with typical method of water treatment

#### **Progress to date**

Experimental: The target ionic liquid tetrabutylphosphonium 5-phenyltetrazolate ([P<sub>4444</sub>][Ph-tet]) has been tested in Crystal16 machine and a standard methodology to measure lower critical solution temperatures of ionic liquids has been set up. In the system, the impact of salinity and pH of water has been explored.

Training: Safety training from CCE research group. NMR machine operation training.

Results: The standard situation for testing in Crystal16 is explored. (optimised SOP for phase determination have been established with 1 ml sample volume, 500 rpm stir rate,  $0.5\text{ }^{\circ}\text{C min}^{-1}$  heating/cooling rate). The impact of pH can not be observed significantly but we can see that the solutions are too acidic and protonation (and precipitation) of the phenyl-tetrazolate anion occurs resulting in we cannot observe the LCST behavior in pH 1 or pH 2 due to protonation and precipitation of the tetrazolate anion. The phase diagram is shown in Figure 1.

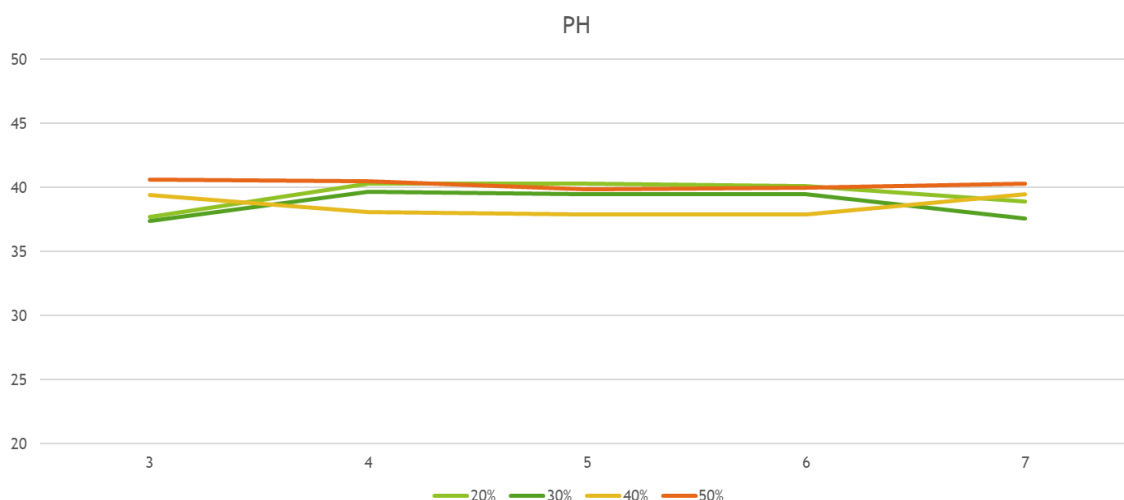


**Figure 1-** Diagrams of different pH and IL concentration temperature / $^{\circ}\text{C}$  on y-axis, pH on x-axis

As for impact of salinity(sodium chloride,g/L), we can significantly observe a decrease trend when we increase the salt concentration of water. It seems like linear relevant which is shown in Figure 2.

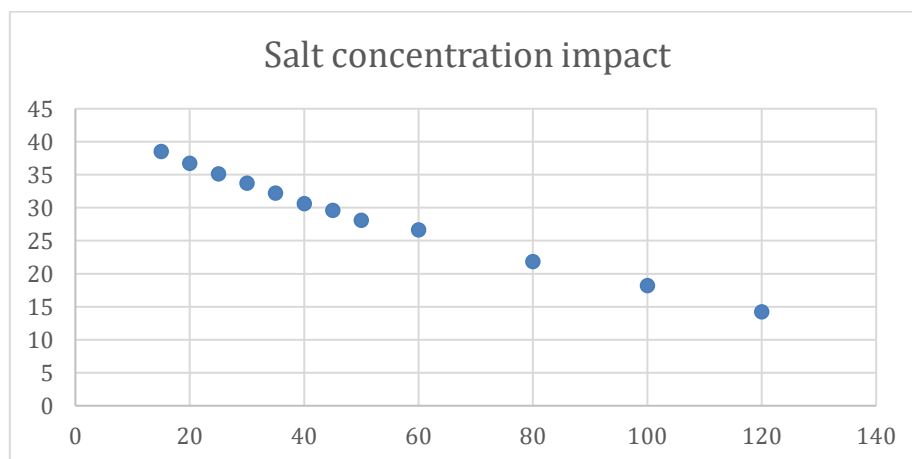


**Figure 2 -** Cloud points under different salt concentration in 40%volume fraction IL concentration temperature / $^{\circ}\text{C}$  on y-axis, salt concentration/ g/L on x-axis-

### Conclusions and future work

In these three months work, a new standard methodology for determining the LCST of ionic liquids has been established by turbidity measurement with optimal conditions determined (1 ml sample volume, over 500 rpm stir rate and  $0.5\text{ }^{\circ}\text{C min}^{-1}$  heating rate). Based on these optimized conditions, we can collect a range of useful data in Crystal16 system including impact of pH and salt content. As for  $[\text{P}_{4444}][\text{Ph-tet}]/\text{water}$  system, we found that higher salt concentration significantly reduce the cloud points of system. However, over the pH range 3-7, there is no obvious impact of pH on the LCST.



In next step, new ionic liquids will be synthesized and characterised based on  $[P_{444}]^+$  cation ionic liquid. I will explore these ionic liquids' phase behaviour and try to optimize them in many ways to select out the best one to inquiry the possibility of its applying in forward osmosis as draw solute. I will also set up a small experimental device for testing forward osmosis.

## QUILL Quarterly Report

Aug 2021 – Oct 2021

<b>Name:</b>	Yaoguang Song		
<b>Supervisor(s):</b>	Prof Peter Nockemann & David Rooney (QUB), Dr Xiaolei Zhang (Strathclyde), Dr Peter Klusener (Shell)		
<b>Position:</b>	PGR Student		
<b>Start date:</b>	3 <sup>rd</sup> Dec 2018	<b>Anticipated end date:</b>	31 <sup>st</sup> May 2022
<b>Funding body:</b>	EU INTERREG VA Programme, managed by SEUPB		

### Thermochemical Conversion of Biomass Lignin into Mesoporous Carbon Materials

#### Background

As a main component, lignin from biomass holds huge potential for producing mesoporous carbons (MCs)<sup>1,2,3</sup>, which represents upper-class valuable products amongst all lignin-based applications.<sup>4</sup> However, most preparation methods for MCs are empirical, leading to unpredictable topologic and structural properties thus likely unfavourable for aimed downstream applications, such as energy storage. Soft-templating synthesis was reported successful to tune nanostructures effectively, but novel promising templates are still in need of development.

A good option is long-chain ionic liquids (ILs) comprised of solely ions, as they can form lyotropic liquid crystals (LLCs), micelles, and (micro) emulsions that have been used for templating synthesis as well. Besides, ILs are also increasingly seen in the dissolution and depolymerisation of lignin. Therefore, this programme aims to investigate the possibility to convert lignin into MCs by employing ILs as both structure-directing agent and solvent. The effective implementation involves both multiscale modelling for computational design of preparation method and tangible experimental validation.

As shown in **Figure 1**, there are several key steps for a successful fabrication of MC by employing ILs as the templates: 1) self-assembly of IL template and carbon precursors; 2) cross-linking of precursors into a stable framework; 3) extraction of IL template; and 4) calcination.

In my previous reports, we studied the self-assembly of ternary mixtures containing IL template, phenolic compounds as precursor, and water as solvent by employing both experiments and multiscale modelling including coarse-grained (CG) molecular dynamics (MD) simulations and density functional theory (DFT) calculations. Results show that ILs as potential template can form hexagonal cylindrical structures in the presence of carbon precursors, which are favourable for the fabrication of MCs. The spatial correlation between IL and phloroglucinol indicates phloroglucinol is a suitable carbon precursor in this case. Then tentative explorations were carried out afterward, though failed to obtain the highly porous carbon materials. During the process, the cross-linking reaction showed huge influence on the formation of porous structures. Before continuing exploring the preparation of MCs by employing IL templates, it is necessary to understand thoroughly the role of cross-linkers. By far, formaldehyde, glyoxal, and glyoxylic acid are three of the most attractive cross-linkers, especially the latter two which are seen as less hazard promising alternatives than formaldehyde. Mayes et al.<sup>5</sup> reported the first time employing glyoxal as cross-linker with

phloroglucinol precursor to prepare MCs, which showed better performance than resorcinol-formaldehyde based MC in capacitive deionisation experiments to treat brackish water. Glyoxal was suggested to stabilise the cross-linking reaction. Herou et al.<sup>6</sup> partly compared the difference of structural morphologies in the porous carbons from glyoxal and glyoxylic acid cross-linkers without taking into account the potential influence of surface functionalities. Therefore, there is still lack of systematic study on how different cross-linking reaction would influence the properties of resultant porous carbons to optimise their energy storage capability. To reveal this thoroughly, this report focuses on the difference both in morphological properties and in surface functionalities of MCs from these 3 most attractive cross-linkers. The overall aim is to shed light on how different cross-linking reactions could influence the pore structures and surface groups, which together could lead to different electrochemical performance when using the resultant carbon materials as electrode materials on supercapacitors.

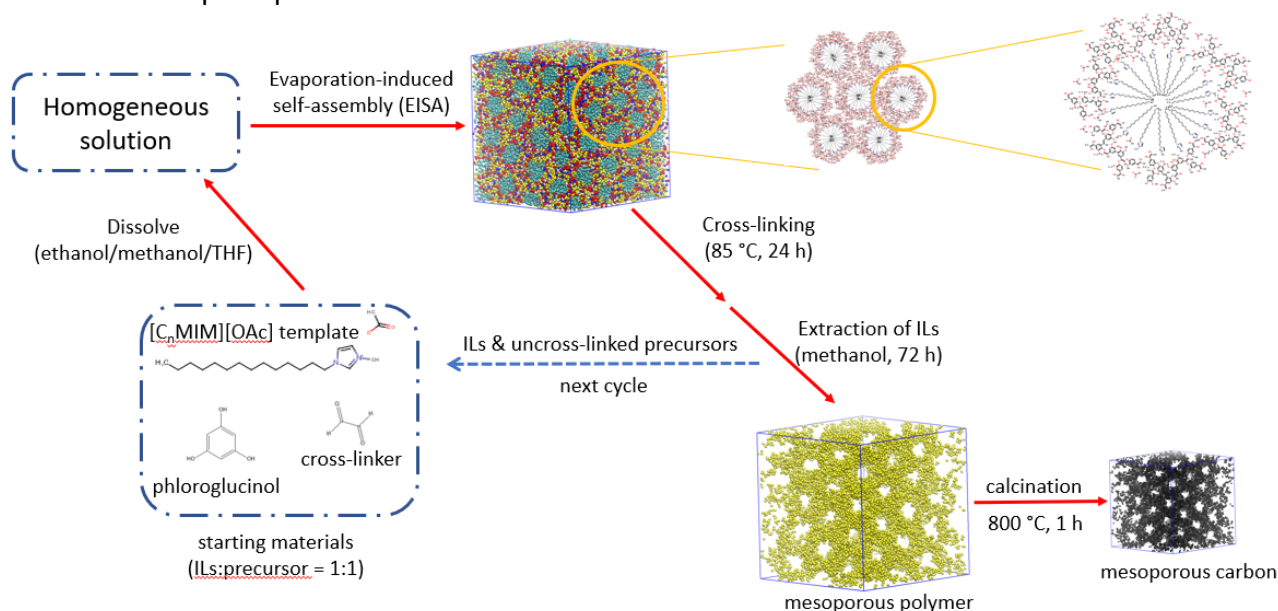


**Figure 1** - Scheme for the fabrication of porous polymer and carbon materials using IL templates

## Methodology

To systematically investigate the role of different cross-linkers on templating synthesis of MCs, a well-established soft template, block copolymer Pluronic F127 was selected to avoid the interfere of IL templates, which may not lead to highly ordered meso-structures.

### 1) Preparation of mesoporous carbons

The preparation process employed an evaporation-induced self-assembly (EISA) technique. For a typical run, 1.71 g of Pluronic F127 and 0.82 g of phloroglucinol were dissolved in 40 mL of absolute ethanol in sequence. After stirring for 30 min, the cross-linking reagent was added dropwise into. The resultant solution was stirred at room temperature for at least 2 h before being poured into a clean smooth glass petri dish and left at 30 °C for 1 day to allow the ethanol to evaporate. After further curing at 85 °C for 1 day, a homogenous transparent thin film was formed which was then chopped into chunks and placed into a quartz boat. The calcination took place under N<sub>2</sub> with a flow rate of 100 mL/min. The polymer was calcinated at 800 °C for 1 h with a heating rate of 1 °C/min, followed by cooling down naturally. The resultant carbon material was labelled as Gx, Fx, and GAx, where G, F, and GA correspond to 3 different cross-linkers: glyoxal (40 wt% aq.), formaldehyde (37 wt% aq.), and glyoxylic acid monohydrate, respectively. The subscript x means the molar ratio of cross-linker/precursor (C/P ratio).



## 2) Characterisation

**Surface area and porosity analysis:** BET surface area and pore volume for samples were analysed by N<sub>2</sub> adsorption-desorption at 77 K under a TriStar II 3020 analyser. Pore size distribution was calculated by BJH method.

**Morphology analysis:** Morphologies of resultant mesoporous carbons were characterised by scanning electron microscopy (SEM) with FEI Quanta 250 FEG (Chemistry) scanning electron microscope, and transmission electron microscopy (TEM) with TALOS F200X G2 microscope; high-angle annular dark-field (HAADF) imaging technique was used for getting scanning transmission electron microscopy (STEM) images.

**Surface functionality analysis:** The organic groups on the surface of resultant MCs were characterised by IR on a PerkinElmer Spectrum 100 FT-IR Spectrometer equipped with a universal ATR sampling accessory. X-ray photoelectron spectroscopy (XPS) will be performed to analyse the surface functionalities.

**Electrochemical performance analysis:** The difference of electrochemical performance of MCs from various cross-linkers will be tested as electrode materials of supercapacitors.

## Results

Figure 2 shows the N<sub>2</sub> physisorption isotherms and pore size distribution for all resultant carbons. The IV type isotherms, the obvious hysteresis loops confirm that all resultant carbon materials have dominating mesopores except GA1.25, which barely showed porosity.<sup>7</sup> GA1 exhibited the largest adsorption quantity with dominating pore size of 8.7 nm; this indicates GA1 has the largest pore volume, followed by sample G1 and F2 with dominating pore size of 6.1 and 8.6 nm, respectively. Also, the adsorption quantity became smaller when the C/P ratio increased. It seems that more cross-linking agents added would bring about smaller porosity at the same condition. Moreover, Figure 2 (b) showed another notable decreasing trend in the dominating pore size of MCs as the increasing C/P ratio. For MCs using glyoxal cross-linker, the dominating pore size decreased from 6.1 nm for G1 to 3.3 nm for G2, while the value dropped to 7.5 nm for GA1.125 for glyoxylic acid cross-linker. Comparing 3 different cross-linkers, pore size distributions for MCs employing glyoxal as cross-linking agent are much narrower than the others, which indicating the mesopores are more uniform and regulated.

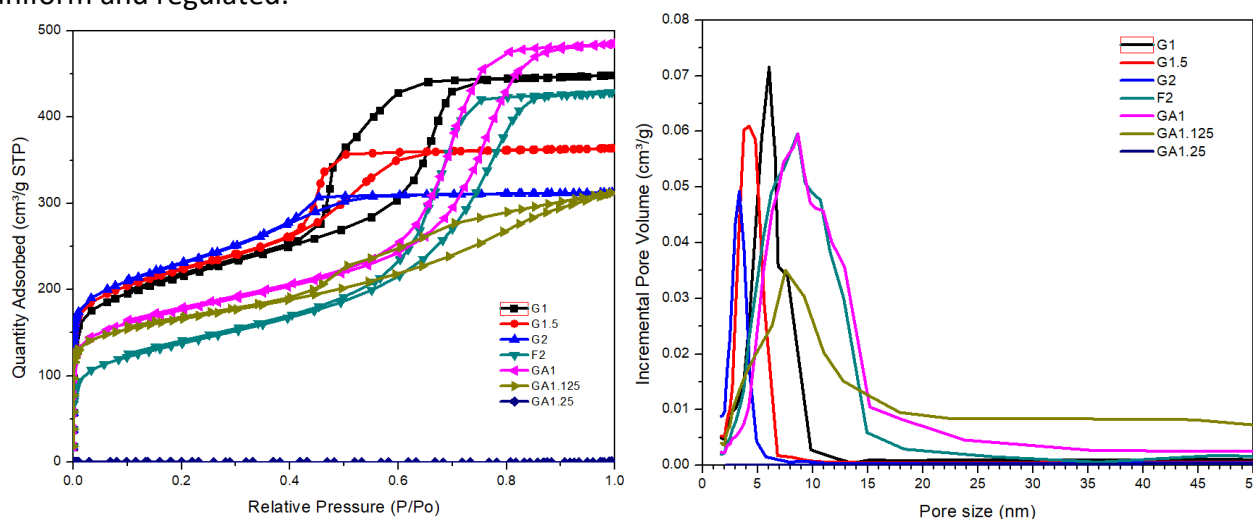


**Figure 2** - N<sub>2</sub> adsorption isotherms (a) and BJH pore size distribution (b) of resultant MCs

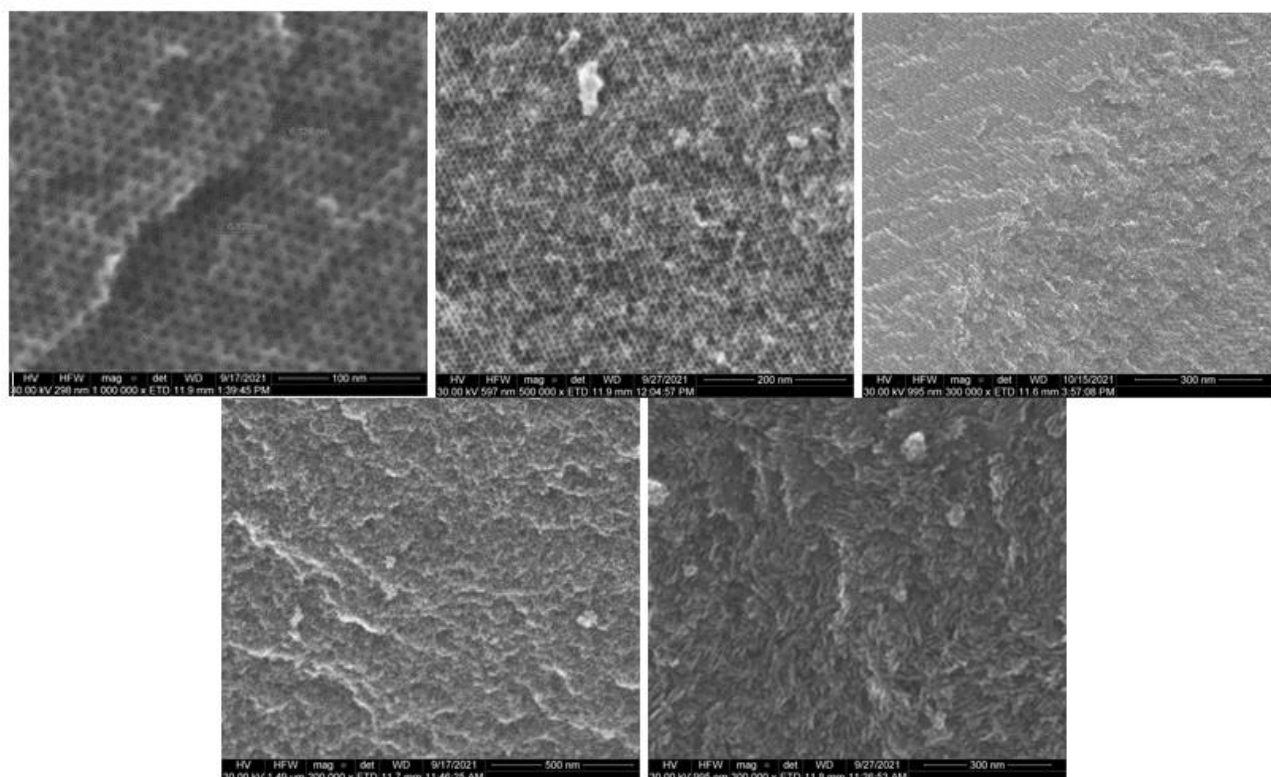
Table 2 summarises the pore textural properties for resultant MCs made by various cross-linkers. MCs with glyoxal as cross-linker showed richer porosity than those with formaldehyde and glyoxylic acid, evidenced by the larger surface area and pore volume. With the increasing C/P ratio, the total surface area increased from 753.4 to 820.7 m<sup>2</sup>/g while the total pore volume decreased from 0.69 to 0.48 cm<sup>3</sup>/g. The mesopore rate dropped notably from 78% to 58 %, which can be associated with the declining mesopore surface area (from 436.3 to 400.0 m<sup>2</sup>/g) and mesopore volume (from 0.54 to 0.28 cm<sup>3</sup>/g). When employing formaldehyde as the cross-linker, the homogenous film could not form after solvent EISA process at lower cross-linker/precursor mixing ratios. This is because that formaldehyde has only 1 aldehyde group; lower formaldehyde/phloroglucinol mixing ratio could lead to deficient cross-linking reaction without catalyst. When the mixing ratio reached 2, the corresponding carbon material F2 showed the highest mesopore rate of 91%. Glyoxylic acid as the cross-linking agent can also provide only 1 aldehyde group per molecule but the carboxyl group can serve as catalyst to facilitate the cross-linking process. However, over-cross-linked precursor could be detached from the hydrophilic segment of templates.<sup>8</sup> Consequently, the porosity became poorer with the increasing of glyoxylic acid and there was barely porosity when the C/P ratio exceeded 1.25. At the same C/P ratio, GA1 exhibited larger total pore volume and mesopore volume than sample G1, which corresponds well with higher N<sub>2</sub> adsorption quantity in Figure 2.

**Table 2** - Textural properties of resultant samples

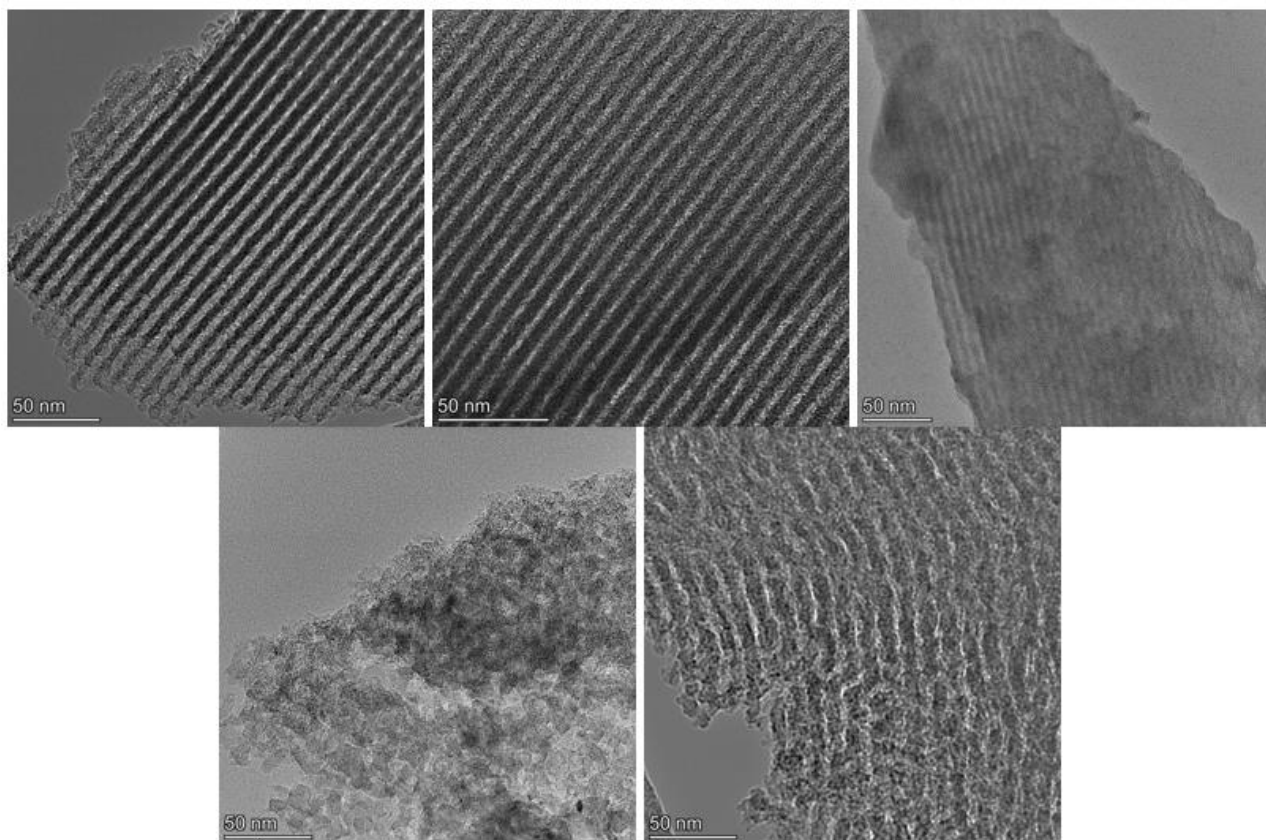
Samples	Pore textural property					dominating pore size (nm)
	$S_{\text{BET}}$ (m <sup>2</sup> /g)	$S_{\text{meso}}$ (m <sup>2</sup> /g)	$V_{\text{total}}$ (cm <sup>3</sup> /g)	$V_{\text{meso}}$ (cm <sup>3</sup> /g)	$V_{\text{meso}}/V_{\text{total}}$	
F2	478.5	367.2	0.66	0.60	91%	8.6
G1	753.4	436.3	0.69	0.54	78%	6.1
G1.5	793.8	423.8	0.56	0.38	68%	4.3
G2	820.7	400.0	0.48	0.28	58%	3.3
GA1	621.7	348.7	0.75	0.62	83%	8.7
GA1.125	597.5	245.6	0.48	0.32	67%	7.5
GA1.25	0.6	0.06	0.0009	0.0008	89%	49

Figure 3-5 shows the representative SEM, TEM, and STEM images of MC samples. MCs with glyoxal cross-linker showed highly ordered hexagonal mesopore structures with a long periodicity. However, formaldehyde as cross-linker led to a randomly disordered mesopore structures, which are the interstitials between polymer clusters. Although the amount of aldehyde groups for F2 is the same with that for G1, the pore structures exhibit so differently. This can be attributed to the higher reactivity of formaldehyde than glyoxal.<sup>5</sup> Sample GA1 showed less ordered mesoporous structures than G1, which can be attributed to the presence of carboxyl group. Compared with formaldehyde at C/P ratio of 1, formaldehyde could not sufficiently cross-link the precursor to form a homogeneous film while glyoxylic acid seems to have resulted the precursor slightly over-cross-linked, evidenced by the less ordered mesopore structures. Periodicity were measured for ordered MCs by STEM HAAFD intensity line profile. As shown in **Figure 5**, the distance between 2 neighbouring peaks means 1 period, which is composed of pore and pore wall. For sample G1, the periodicity was 10.5 nm with a pore size and pore wall of 6.1 and 4.4 nm, respectively. As the C/P ratio increased to 1.5, the periodicity decreased to 8.7 nm, where the pore size shrunk to 4.3 nm. Sample G2 showed a smaller periodicity of 8.2 nm with a narrower pore diameter of 3.3 nm. The

pore diameters measured correspond exactly to the dominating pore sizes from N<sub>2</sub> adsorption analysis. However, for sample GA1 with a less ordered pore structure, the periodicity was 12.5 nm, larger than other ordered samples. The measured average pore diameter from microscope was 5.4 nm, which is smaller than the dominating pore size from N<sub>2</sub> adsorption analysis. This could be caused by the distortion of pore channel and the discontinuity of pore walls.



**Figure 3** - SEM images of samples: G1, G1.5, G2, F2, and GA1, respectively



**Figure 4** - TEM images of samples: G1, G1.5, G2, F2, and GA1, respectively



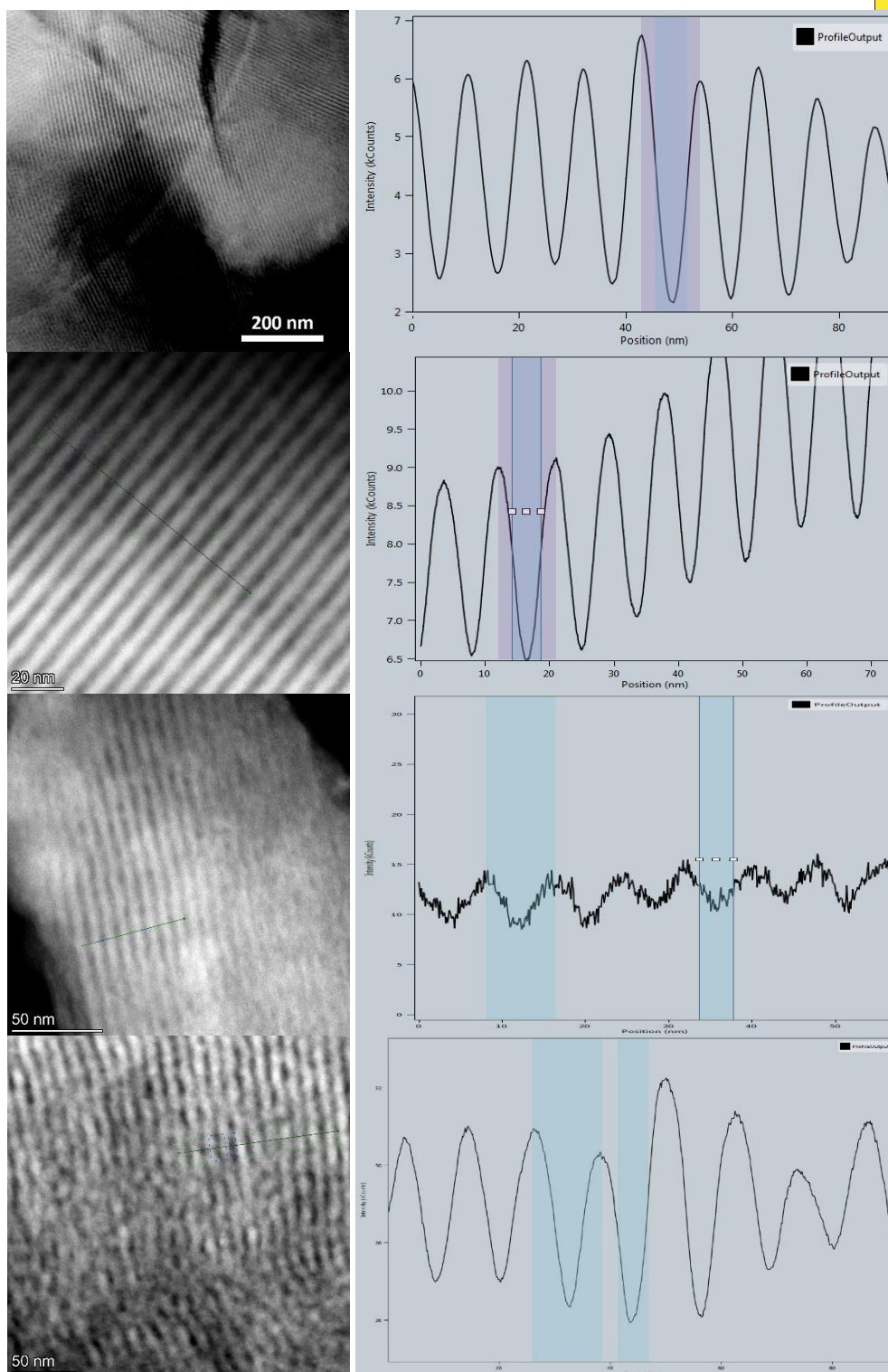


**Figure 5** - HA-ADF STEM image and line profile of processed HA-ADF intensity for ordered mesoporous samples: G1, G1.5, G2, GA1, respectively

The surface functionality was characterised by IR. As shown in Figure 6(a), the band observed at around  $1560$  and  $1020\text{ cm}^{-1}$  are characteristic of  $\text{-C=O}$  group and  $\text{-C-O}$  group, respectively.<sup>9</sup> With the increasing of C/P ratio, the peak for  $\text{-C-O}$  group became higher whilst  $\text{-C=O}$  group showed a converse trend. This is associated with the cleavage of  $\text{-C=O}$  bond during the addition of glyoxal to aromatic precursors, consequently a new  $\text{-C-O}$  bond will form after the reaction leading to an increasing content of  $\text{-C-O}$  group. When employing glyoxylic acid as the cross-liner, the peak of  $\text{-C=O}$  group remained similar with that in sample G1 while the peak of  $\text{-C-O}$  group became higher. Due to the

presence of carboxyl group in glyoxylic acid, which provides 2 -C=O bonds and 1 -C-O bond, the carboxyl group remained after the cross-linking reaction as it only acted as the catalyst. Double moles of formaldehyde give the same amount of aldehyde group as glyoxal, but the peak for -C-O group became lower than those in sample G1. As formaldehyde is a faster reacting cross-linking agent, it could easily bridge 2 polymer monomers and form -CH<sub>2</sub>- group. Therefore, the content of -C-O became much lower. To quantify the detailed content of each functionality, XPS will be performed.

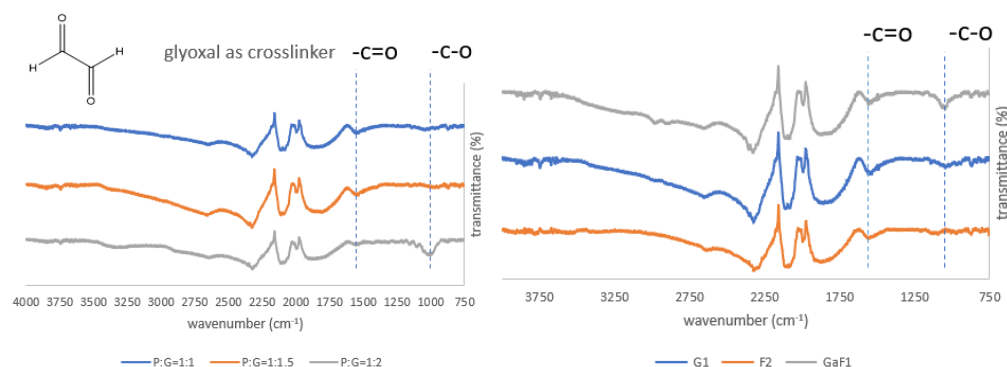


**Figure 6** - IR spectra of resultant samples: a) G series, and b) comparison

### Conclusions and future work

The role of cross-linking reaction on the resultant mesopore structure and surface functionality of MCs was studied. Glyoxal proves to be a greener promising cross-linker, leading to a highly ordered uniform hexagonal mesopores. Mesopores can be tuned from 3.3 and 6.1 nm as the cross-linker/precursor ratio decreases. Glyoxylic acid and formaldehyde could bring about over-cross-linked precursor, which would destabilise the ordered mesophase and result in less ordered or disordered pore structures.

In the future, surface functionalities of materials will be investigated in detail. The supercapacitor cell has been printed with Ultimaker 3D printer. The difference in electrochemical performance of materials from different cross-linkers will be studied. The potential use of amphiphilic ILs as templates will continue being studied with glyoxal as cross-linker.

### References

- 1 D. Montané, V. Torné-Fernández and V. Fierro, *Chem. Eng. J.*, 2005, **106**, 1–12.
- 2 Y. Song, J. Liu, K. Sun and W. Xu, *RSC Adv.*, 2017, **7**, 48324–48332.
- 3 J. M. Rosas, R. Berenguer, M. J. Valero-Romero, J. Rodríguez-Mirasol and T. Cordero, *Front. Mater.*, , DOI:10.3389/fmats.2014.00029.
- 4 A. M. Puziy, O. I. Poddubnaya and O. Sevastyanova, *Top. Curr. Chem.*, 2018.
- 5 R. T. Mayes, C. Tsouris, J. O. Kiggans, S. M. Mahurin, D. W. Depaoli and S. Dai, *J. Mater. Chem.*, 2010, **20**, 8674–8678.
- 6 S. Herou, M. C. Ribadeneyra, R. Madhu, V. Araullo-Peters, A. Jensen, P. Schlee and M. Titirici, *Green Chem.*, 2019, **21**, 550–559.
- 7 M. Thommes, K. Kaneko, A. V. Neimark, J. P. Olivier, F. Rodriguez-Reinoso, J. Rouquerol and K. S. W. Sing, *Pure Appl. Chem.*, 2015, **87**, 1051–1069.
- 8 D. Saha, R. Zacharia and A. K. Naskar, in *ACS Symposium Series*, 2014, vol. 1173, pp. 61–83.
- 9 H. N. Tran, F. C. Huang, C. K. Lee and H. P. Chao, *Green Process. Synth.*, 2017, **6**, 565–576.



## QUILL Quarterly Report

August 2021 – October 2021

<b>Name:</b>	Richard Woodfield		
<b>Supervisor(s):</b>	Dr Stephen Glover, Dr Robert Watson and Prof Peter Nockemann		
<b>Position:</b>	PhD Student		
<b>Start date:</b>	06/2019	<b>Anticipated end date:</b>	12/2022
<b>Funding body:</b>	EPSRC		

### Modelling the use of Flow Batteries in Transport Applications

#### Background

Flow batteries have received significant attention in the past years for use in grid storage applications. The decoupling of the relationship between power and energy density offers a very unique way to store energy to suit the user's particular needs. The extremely long cycle life of a flow-battery is another attractive asset, as the electrodes do not undergo cyclic stressing in the same way Li-ion and other chemistries do. Flow-batteries have received very limited attention regarding their use in transport applications. There is untapped potential in the fact that the discharged electrolyte of a flow-battery could be rapidly swapped at a traditional gas-station, where the infrastructure is already half in-place with storage tanks under the stations. With the electrolyte being entirely re-usable, the station would use an on-site flow-battery to recharge their reservoir and provide passing vehicles with opportunity to swap their electrolyte with readily charged fluid.

#### Objective of this work

The overall goal of the project is to identify viable electric or hybrid modes of transport that would benefit from the use of a flow-battery, given the refillable nature of the flow-battery electrolyte reservoirs. Even the applications rendered not viable will have outcomes, as the amount by which the energy density of the electrolyte would need to improve by is also providing electrolyte chemists with targets to aim for. The investigations will be carried out using software to model battery and vehicle behaviour, primarily Simulink.

#### Progress to date

Modelling work has shown that coastal ferries are a very good candidate for RFB technology, and a paper has been submitted in this area.

#### Conclusions and future work

Modelling work is now shifting towards bus applications, exploring a range of system architectures and control strategies.



## QUILL Quarterly Report

February 2021 – April 2021

<b>Name:</b>	John (Mark) Young		
<b>Supervisor(s):</b>	Dr Leila Moura, Prof John Holbrey and Prof Sophie Fourmentin		
<b>Position:</b>	PhD student		
<b>Start date:</b>	2020	<b>Anticipated end date:</b>	2024
<b>Funding body:</b>	EPSRC		

### Gas separation technologies

#### 1.1 Background

Biogas is a renewable and carbon neutral energy source obtained through anaerobic digestion (AD) of organic waste. Biomethane is obtained through the upgrading of biogas produced from anaerobic digestors. It consists of mainly methane and carbon dioxide with many trace compounds including hydrogen sulfide, ammonia, siloxanes, terpenes and water vapour. Biomethane must be of a purity equal to or better than that of natural gas if it is to be utilised for grid injection therefore a methane purity of above 96% must be achievable from any prospective technology. Carbon dioxide should make up 2.5-4% of the remaining volume with contaminants such as sulfur and siloxanes being limited to 10 mg/m<sup>3</sup> and 0.1 mg/m<sup>3</sup> respectively. Due to the major biogas components being carbon dioxide and methane it is this separation we will focus on in this project.<sup>1</sup>

Currently biogas upgrading is multistep and scrubbing is mainly used for carbon dioxide and methane separation. This involves the use of liquid amines where the carbon dioxide uptake occurs through a chemisorption process. This requires high energy for amine regeneration in the form of steam at 100-150°C to reform the initial liquid amine. Water scrubbing can also be used but this requires vast amounts of water and leads to methane slip due to the lower selectivity of water compared with other technologies. Membranes offer another option for upgrading but these also suffer from a range of issues such as a low throughput coupled with fouling and plasticisation. The degradation of membranes leads to issues both economically in the form of having to replace them but from an environmental standpoint it is unsustainable to continuously have to dispose of and manufacture replacement membranes. Cryogenic distillation offers a method of using nontoxic materials to produce high purity gas streams through the utilisation of low temperatures and high pressures which allows carbon dioxide to liquify leaving a pure methane stream. However the energy cost associated with this method is massive which makes it less sustainable and exceedingly costly.<sup>2</sup>

It is for these reasons that we seek to create novel materials which will be more efficient, more sustainable and economically viable. Initial work will consist of the use of deep eutectic solvents in conjunction with other sorbents to increase their upgrading capabilities.

#### 1.2 Work to date

The screening methodology has improved since previous reports with the utilization of our own recently repaired HS-GC. This has increased the maximum screening pressure to around 3 bar which is substantially higher than the previous report of 1.8 bar.



My project currently centres around the testing of low melting mixtures (LMMs) in conjunction with dissolved macrocycles such as cyclodextrin(CD) and cucurbituril(CB). It is hoped that these dissolved macrocycles will enhance the uptake capacity and selectivity for CO<sub>2</sub> of the LMMs through host guest chemistry. Materials synthesis and subsequent testing has been my major focus since the last quarterly report. CO<sub>2</sub> uptake results for [Ch]Cl:U 1:2 with the addition of beta CD can be seen in figure 1. This shows that the addition of 9.1 wt% beta CD increases the uptake capacity of [Ch]Cl:U 1:2 by almost 100%. It is thought this increased uptake is brought about through host guest chemistry of the CO<sub>2</sub> entering the cavity of the CD. Similar behaviour is found with the addition of the larger 7 membered gamma CD where we get very similar increase in CO<sub>2</sub> uptake capacity over pure [Ch]Cl:U 1:2.

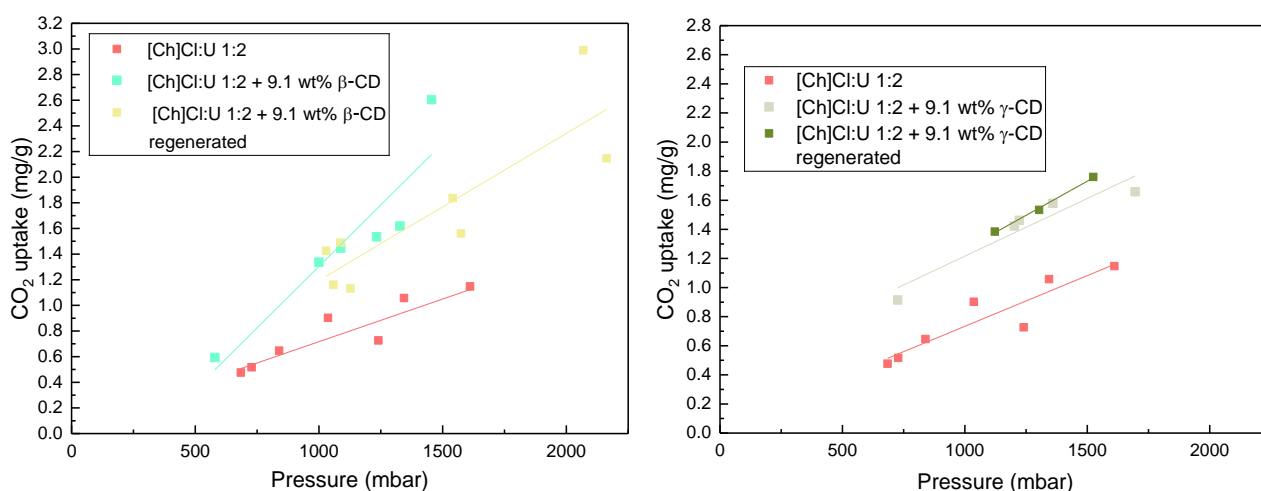


**Figure 1** - CO<sub>2</sub> uptake graphs comparing [Ch]Cl:U 1:2 with and without the addition of beta CD (left) and gamma CD (right) where regeneration was carried out by removing CO<sub>2</sub> from dissolved samples using vacuum before retesting capacity

The same behaviour was not seen upon the addition of alpha CD to choline chloride:urea ([Ch]Cl:U) 1:2 as can be seen in figure 2. The uptake capacity remains approximately the same for both samples. The cause for this is not yet known but we hope to elucidate this through NMR based experiments.

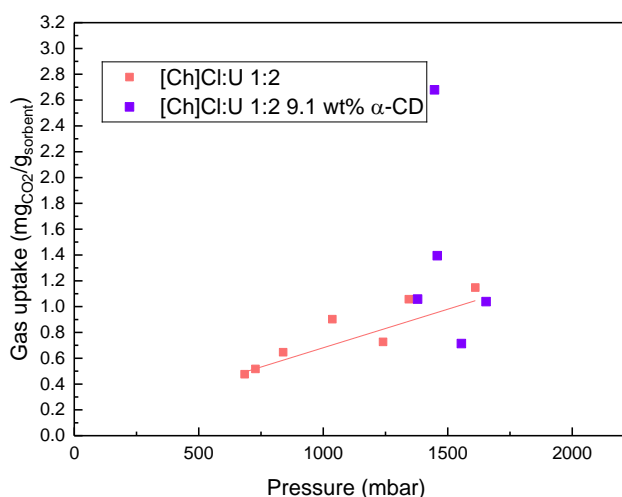


**Figure 2** - CO<sub>2</sub> uptake graphs comparing [Ch]Cl:U 1:2 with and without the addition of alpha CD

Work has also been carried out investigating the CO<sub>2</sub> uptake capacity of trioctylphosphine oxide:phenol (TOPO:Phenol) based materials. Preliminary measurements seen in figure 3 show a large uptake capacity of this material. This uptake is within the range found with one of the best physisorbant ionic liquids 1-Butyl-3-methylimidazolium bis(trifluoromethylsulfonyl)imide([Bmim][NTf<sub>2</sub>]). This uptake is not commonly found in physisorbant materials without the use of fluorination so is incredibly interesting for our measurements. All or most of this CO<sub>2</sub> is thought to be physisorbed and not chemisorbed due to the presence of a characteristic CO<sub>2</sub> peak found in NMR experiments with no peak attributed to carbonate formation from reaction of phenol with CO<sub>2</sub>.<sup>3</sup>

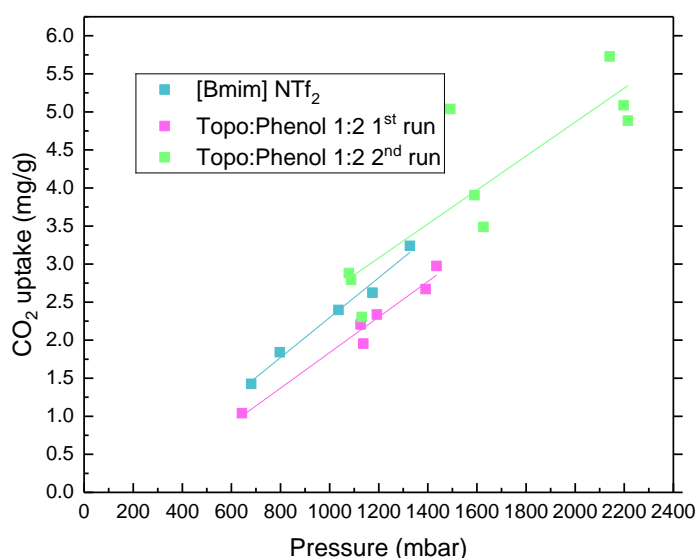


**Figure 3** - CO<sub>2</sub> uptake graphs comparing Topo:Phenol uptakes to that of [Bmim][NTf<sub>2</sub>]

### 1.3 Future work

Future work will be to test all material's uptake capacities with pure CH<sub>4</sub> and with 50/50 CO<sub>2</sub>/CH<sub>4</sub> gas mixtures to find the selectivity of all materials. This will give insight into their feasibility to be used for biogas upgrading. NMR experiments will also be used in order to try to confirm the host guest chemistry between gas and macrocycles. Switching of phenol to a greener component such as catechol will also be tested in order to synthesise a more environmentally benign material while keeping the high capacity for CO<sub>2</sub>. Tests will also be carried out with dissolution of macrocycles in TOPO based DES.

### References

- 1 F. M. Baena-Moreno, M. Rodríguez-Galán, F. Vega, L. F. Vilches and B. Navarrete, *Int. J. Green Energy*, 2019, **16**, 401–412.
- 2 M. R. Rodero, R. Ángeles, D. Marín, I. Díaz, A. Colzi, E. Posadas, R. Lebrero and R. Muñoz, in *Biogas*, Springer, 2018, pp. 239–276.
- 3 H. Yan, L. Zhao, Y. Bai, F. Li, H. Dong, H. Wang, X. Zhang and S. Zeng, *ACS Sustain. Chem. Eng.*, 2020, **8**, 2523–2530.